MAPPING THE LANDSCAPE OF ACQUIRED VULNERABILITIES IN OVARIAN CANCER

APPROVED BY SUPERVISORY COMMITTEE

Dr. Michael White, Ph.D.

Dr. Steven Altschuler, Ph.D.

Dr. Rolf Brekken, Ph.D.

Dr. Diego Castrillon, M.D., Ph.D.

DEDICATION

I would like to thank the members of my Graduate Committee, members of the White Lab, and the MSTP program for all of their support. I would especially like to thank my mentor Dr. Michael White. Most of all I would like to thank my parents, Joel and Regina Shields, and my girlfriend, Courtney Robertson, for their endless patience and support.

MAPPING THE LANDSCAPE OF ACQUIRED VULNERABILITIES IN OVARIAN CANCER

by

BENJAMIN BAKER SHIELDS

DISSERTATION

Presented to the Faculty of the Graduate School of Biomedical Sciences

The University of Texas Southwestern Medical Center at Dallas

In Partial Fulfillment of the Requirements

For the Degree of

DOCTOR OF PHILOSOPHY

The University of Texas Southwestern Medical Center at Dallas

Dallas, Texas

May, 2013

MAPPING THE LANDSCAPE OF ACQUIRED VULNERABILITIES IN OVARIAN CANCER

Publication No._____

Benjamin Baker Shields, Ph.D.
The University of Texas Southwestern Medical Center at Dallas, 2013

Supervising Professor: Dr. Michael White, Ph.D.

Recent undertakings to identify the genetic lesions associated with ovarian cancer have noted the striking diversity of mutations occurring in this disease. This genetic diversity has complicated the search for novel therapies. However, recent data has suggested that one commonality of ovarian tumors might be ablation of miRNA biogenesis. Here I conducted a broad-scale gain-of-function microRNA (miRNA) screen in 16 ovarian cancer cell lines to annotate the functional landscape present in such a chaotic genetic background. miRNAs function as multigenic perturbations allowing for interrogation of maximal gene space with few experiments. This screen identified multiple miRNAs reducing cell viability with the majority of

hits being toxic in only one or two lines screened. This surprising finding reflected the commonality of altered miRNA function in ovarian tumors while also suggesting that specifics of this alteration in function are unique to each tumor. To investigate more public vulnerabilities, I focused mechanistic studies on miRNAs displaying penetrance in greater than 5 cell lines. miR-517a reduced cell viability in over 30% of the panel and also reduced tumor burden in vivo. Functional analysis of the predicted targets of miR-517a revealed that expression of this miRNA reduced protein levels of ARCN1, a member of the coatamer complex, and that knockdown of ARCN1 reduced cell viability similar to miR-517a. Another penetrant miRNA, miR-124a, reduced cell viability in 37.5% of the panel and functional analysis of this miRNA revealed it promoted a cell differentiation program. Analysis of predicted targets revealed that expression of miR-124a reduced expression the homeodomain transcription factor SIX4, resulting in increased signaling along the tumor suppressive AMPK pathway and epithelial differentiation. Furthermore, SIX4 displayed increased expression in ovarian tumors and depletion of SIX4 expression reduced tumor cell viability in vitro and in vivo. Therefore, SIX4 overexpression might function to deflect cell differentiation in tumors. Thus, the common loss of miRNA function observed in ovarian tumors might serve to maintain an undifferentiated state, and engagement of cell fate determination programs via re-expression of miRNAs can result in catastrophic consequences for cancer cell viability.

TABLE OF CONTENTS

PRIOR PUBLICATIONS

None

LIST OF FIGURES

LIST OF APPENDICES

LIST OF DEFINITIONS

3’-UTR – 3’ untranslated region

ACC – Acetyl CoA carboxylase

AKT – v-akt murine thymoma viral oncogene homolog

AKT1 – v-akt murine thymoma viral oncogene homolog 1

AKT2 – v-akt murine thymoma viral oncogene homolog 2

AKT3 – v-akt murine thymoma viral oncogene homolog 3

AMPK – AMP-activated protein kinase

APML – Acute promyelocytic leukemia

AR – Androgen receptor

ARCN1 – Archain 1

ATRA – All-trans retinoic acid

BRAF – v-raf murine sarcoma viral oncogene homolog B1

BRCA1 – Breast cancer 1, early onset

BRCA2 – Breast cancer 2, early onset

BrdU – 5-bromo-2-deoxyuridine

CBLC – Cbl proto-oncogene, E3 ubiquitin protein ligase C

CCNE1 – Cyclin E1

CDH2 – Cadherin 2, type 1, N-cadherin (neuronal)

CDK12 – Cyclin-dependent kinase 12

CDK6 – Cyclin-dependent kinase 6

ChIP-Seq – Chromatin immunoprecipitation followed by next generation sequencing

CNV – Copy number variation

CSMD3 – CUB and Sushi multiple domains 3

CTNNB1 – Catenin (cadherin-associated protein), beta 1, 88kDa

DGCR8 – DiGeorge syndrome critical region gene 8

DICER1 – Dicer 1, ribonuclease, type III

DNA – Deoxyribonucleic acid

DOPC – 1,2-dioleoyl-sn-glycero-3-phosphatidylcholine

DROSHA – Drosha, ribonuclease type III

ds-miRNA – Double-stranded miRNA mimic, such as those from Dharmacon

EMT – Epithelial-to-mesenchymal transition

EOC – Epithelial Ovarian Cancer

EPHB1 – Eph receptor B1

EYA – Eyes absent homolog

EYA1 – Eyes absent homolog 1

EYA2 – Eyes absent homolog 2

EYA3 – Eyes absent homolog 3

EYA4 – Eyes absent homolog 4

FAT3 – FAT tumor suppressor homolog 3 (Drosophila)

FOXM1 – Forkhead box M1

FRAP1 – Mechanistic target of rapamycin (MTOR), serine/threonine kinase

G1 – Growth phase 1

G12D RAS – Constitutively active RAS mutant

GABRA6 – Gamma-aminobutyric acid (GABA) A receptor, alpha 6

GAP – GTPase activating protein

HOSE – Human ovarian surface epithelium

ID proteins – Inhibitor of DNA binding proteins (ID1, ID2, and ID3)

ID1 – Inhibitor of DNA binding 1, dominant negative helix-loop-helix protein

ID2 – Inhibitor of DNA binding 2, dominant negative helix-loop-helix protein

IHH – Immortalize human hepatocytes

IL6 – Interleukin 6 (interferon, beta 2)

IP - Immunoprecipitation

IRAK1 – Interleukin-1 receptor-associated kinase 1

ITPR3 – Inositol-1,4,5-triphosphate receptor, type 3

KRAS – v-Ki-ras2 Kirsten rat sarcoma viral oncogene homolog

KREMEN1 – Kringle containing transmembrane protein 1

LKB1 – Serine/threonine kinase 11 (STK11)

LNA – Locked nucleic acid

MAP2 – Microtubule-associated protein 2

MAPK – Mitogen activated protein kinase

MAS1L – MAS1 oncogene-like

MECOM – MDS1 and EVI1 complex locus

miRNA – microRNA

MO25 – Calcium binding protein 39 (CAB39)

MYC – v-myc myelocytomatosis viral oncogene homolog (avian)

NF1 – Neurofibromin 1

NFKBIZ – Nuclear factor of kappa light polypeptide gene enhancer in B-cells inhibitor, zeta

NFκB – Nuclear factor kappa B

NSCLC – Non-small cell lung cancer

p21 – Gene product of cyclin-dependent kinase inhibitor 1A locus

p53 – Gene product of tumor protein p53 locus

PAX8 – Paired box 8

PI3K – Phosphatidylinositol-4,5-bisphosphate 3-kinase

PIK3CA – Phosphatidylinositol-4,5-bisphosphate 3-kinase, catalytic subunit alpha

PKHD1 – Polycystic kidney and hepatic disease 1 (autosomal recessive)

pre-miRNA – miRNA that has been processed by Drosha but not Dicer

pri-miRNA – Unprocessed primary miRNA

PTB – Polypyrimidine tract binding protein 1 (PTBP1)

PTEN – Phosphatase and tensin homolog

PTK7 – Protein tyrosine kinase 7

RAS – Rat sarcoma viral oncogene homolog

RB1 – Retinoblastoma 1

REST – RE1-silencing transcription factor

RISC – RNA-induced silencing complex

RNA – Ribonucleic acid

SCNA – Somatic copy number alteration

SCP1 – CTD (carboxy-terminal domain, RNA polymerase II, polypeptide A) small phosphatase 1

siRNA – small interfering RNA

SIX – SIX (sine oculis) homeobox homolog

SIX4 – SIX homeobox 4

SMAD – Mothers against decapentaplegic homolog

SMAD2 – SMAD family member 2

SMAD3 – SMAD family member 3

SMAD4 – SMAD family member 4

SMURF2 – SMAD specific E3 ubiquitin protein ligase 2

SNV – single nucleotide variation

ss-LNA – Single-stranded miRNA mimic using LNA technology

ss-siRNA – Single-stranded siRNA using LNA technology

STRADA – STE20-related kinase adaptor alpha

STRADB – STE20-related kinase adaptor beta

TCGA – The Cancer Genome Atlas

TERT – telomerase reverse transcriptase

TGFβ – Transforming growth factor beta

TP53 – Tumor protein p53

TRAF6 – TNF receptor-associated factor 6, E3 ubiquitin protein ligase

TUBB3 – Tubulin, beta 3 class III

USP1 – Ubiquitin specific peptidase 1

VAMP2 – vesicle-associated membrane protein 2 (synaptobrevin 2)

ZEB1 – Zinc finger E-box binding homeobox 1

ZEB2 – Zinc finger E-box binding homeobox 2

CHAPTER ONE
Introduction

Epithelial ovarian cancer (EOC) accounts for the vast majority of malignant tumors arising in the ovary. Poor outcomes have dictated a need to search for new treatments of this disease, and a greater understanding of the biology driving this disease is required for the development of novel therapies. My project focused on exploring some of the biological consequences of the dysregulated growth of ovarian cancer cells. In order to progress, a cancer must disregard or inactivate pathways and checkpoints evolved to prevent the unregulated, limitless growth observed in cancer cells. These alterations to the cell machinery lead to addiction to other pathways and acquisition of vulnerabilities not found in normal, regulated cells. My project utilized microRNA (miRNA) mimics to survey these vulnerabilities in hopes of uncovering novel biology underlying ovarian cancer. The following introduction focuses first on describing the clinical aspects of ovarian cancer and then on some of the relevant known biology of the disease. Following that, a description of miRNA function and its possible role in ovarian cancer is presented to provide a gateway into my project.

1.1 Ovarian Cancer and the Urgent Need for New Therapeutic Opportunities

Because ovarian cancer is the most lethal gynecologic cancer in the developed world, there is an urgent need for new therapies to treat this disease (Levin, 2008; Siegel et al., 2012). Ovarian cancer is disproportionately lethal in the United States. It is the ninth most common cancer diagnosed in women but the fifth most deadly (Siegel et al., 2012). Many different facets

of the disease are believed to drive this unbalanced lethality. First, treatment of the disease has not appreciably advanced since the late-1970s. Breakthroughs in treatment have been limited to empirical optimization of traditional chemotherapeutics. Furthermore, the combinations of drugs used today are incredibly similar to those used in the mid-1970s with advances in drug delivery allowing for higher achievable concentrations with fewer adverse affects (Vaughan et al., 2011). One improvement is intraperitoneal delivery of drugs, allowing for exposure of higher concentrations of drug to the site of disease if patients can withstand increased adverse effects associated with the treatment (Armstrong et al., 2006; Tournigand et al., 2003). Finally, increasing the quality of surgical care has improved overall patient treatment. In fact, the effectiveness of a patient's surgery is currently the largest determinant of prognosis outside of disease stage at diagnosis (Aletti et al., 2006; Eisenkop et al., 2003).

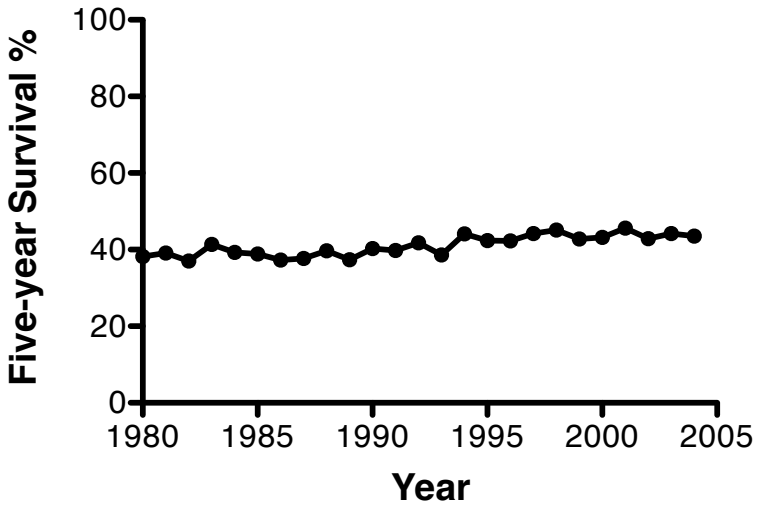

Figure 1.1 The 5-year survival rate for ovarian cancer has not appreciably increased in the past 25 years.

The minimal gains in treatment options are mirrored in the minimal gains in the five-year survival of ovarian cancer patients over the past twenty-five years (Figure 1.1). Though the 5-year survival of all patients diagnosed with ovarian cancer is currently 43.7%, this rate is inflated by the relatively good survival rates of patients diagnosed with early stage disease (Stage I/II). These patients have 5-year survival rates of greater than 90% and 75% for stage I and II respectively (Howlander N, 2012). However, almost two-thirds of patients are diagnosed with advanced, metastatic disease (Stage III/IV), which carries a much worse prognosis (Figure 2). Similar to patients with advanced cancer at other anatomical sites, patients with a Stage III/IV diagnosis have a poor 5-year survival of less than 30%; much lower than their early stage counterparts (Figure 1.2) (Howlander N, 2012). One reason for this large portion of patients receiving late diagnoses is that the relatively bland cohort of symptoms accompanying ovarian cancer (such as abdominal pain or bloating, urinary symptoms, fatigue, and early satiety) mimics common gastrointestinal and genitourinary issues. Though often termed a "silent killer," almost all patients experience symptoms prior to diagnosis (Goff et al., 2000). Importantly, overall cure rates of the disease have not improved from around 30% in the past twenty-five years (Howlander N, 2012; Vaughan et al., 2011). These statistics suggest that while modest improvements in five-year survival have been achievable through empirical optimization of traditional chemotherapy and increased effectiveness of surgery, true improvement to treatment of this disease will only be achieved with new therapies derived from a better understanding of the biology underlying and driving ovarian cancer.

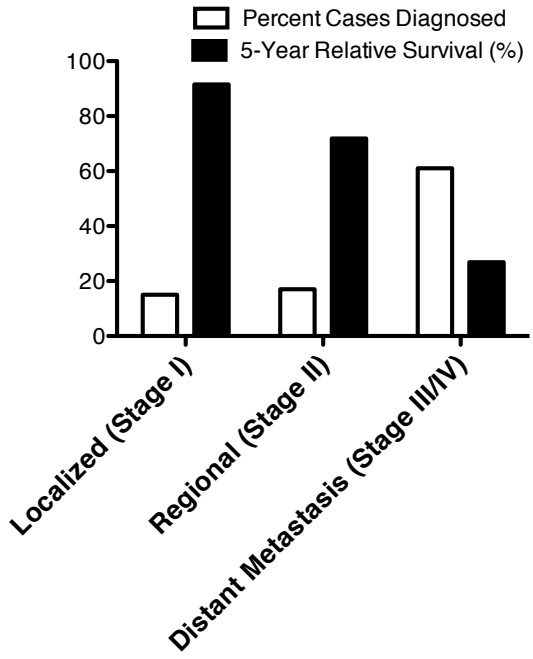

Figure 1.2. The majority of ovarian cancer cases are diagnosed at late stage with a poor prognosis.

1.2 Chemoresistance in Ovarian Cancer

Almost universal resistance to traditional chemotherapeutics further complicates the current treatment modalities of ovarian cancer. The majority of ovarian cancer patients will respond to the current standard treatment combination of platinum and taxanes, with no detectable residual disease in many patients (Bast et al., 2009). However, small numbers of drug resistant cancer cells can survive current treatments and remain dormant. This minor population of drug-resistant cells grows progressively until the patient's disease is resistant to the treatments currently available in the clinic. An increased understanding of the mechanisms leading to

chemoresistance will certainly uncover new methods of restoring sensitivity to current drugs or targeting vulnerabilities linked to drug-resistance.

One feature currently thought to be driving the broad chemoresistance seen in ovarian cancer is the extreme amount of heterogeneity existing within the disease both histologically and genetically. An increased focus on identifying the cell of origin of ovarian cancer has lead to an emerging hypothesis that ovarian cancer is, in fact, many diseases at one site. The common feature belonging to all ovarian cancers is the appearance of a pelvic, peritoneal mass. Differing histological subtypes, previously thought to be different manifestations of the same disease, are now beginning to be thought of as distinct diseases sharing a single site. As an example, the majority of mucinous adenocarcinomas of the ovary are now thought to arise elsewhere in the gastrointestinal tract namely, the appendix (Kelemen and Kobel, 2011; Storms et al., 2012; Zaino et al., 2011). Additionally, endometrioid and clear cell carcinomas of the ovary appear to share similar molecular lesions with endometrial carcinomas and may arise from foci of endometriosis within the ovary (Ayhan et al., 2012; Guan et al., 2011; Jones et al., 2010; Wiegand et al., 2010; Wu et al., 2012).

Moreover, the major subtype of ovarian cancer, serous ovarian adenocarcinoma, is currently postulated to have two possible cells of origin, the epithelial cells covering the ovary and epithelial cells of the fallopian tubes (Folkins et al., 2009; Jarboe et al., 2008; Kindelberger et al., 2007; Levanon et al., 2010). A mouse model of ovarian cancer recently observed that tumors arise in animals that have their ovaries resected, but not those with the fallopian tubes resected (Kim et al., 2012). Other work in mice has recently identified a putative ovarian stem

cell niche that appears to be susceptible to tumorigenic transformation, and might prove to be the cell of origin for some epithelial ovarian cancers (Flesken-Nikitin et al., 2013). The significance of oviductal epithelial cells versus ovarian surface epithelial cells as the cell of origin for the most common epithelial ovarian cancer is still unclear.

Additional investigations into the functional and genetic differences between the subtypes of EOC will allow for more tailored and more effective therapies, as currently all ovarian cancer patients receive the same therapy. Genetic studies of these different subtypes have observed differing constellations of mutations for each subtype, further suggesting functional differences between these subtypes (Tothill et al., 2008). More studies are required to determine whether these tumors are truly multiple diseases at the same site or different manifestations of the same disease. If these are truly different diseases, increased understanding of their origins, similarities, and differences will allow for improved design of clinical trials and more rational design of new treatment regimens.

1.3 Genetic and Molecular Lesions in Ovarian Cancer

In addition to histological heterogeneity, genetic heterogeneity appears to be a common theme for ovarian tumors. This heterogeneity appears to exist not only between different patients' tumors but also within a single patients tumor. The need for a greater understanding of the molecular underpinnings of ovarian cancer has led to multiple broad scale studies to investigate the genetics of ovarian tumors. Two major efforts have been made to sequence ovarian tumors to explore the mutational space of this cancer (Cancer Genome Atlas Research,

2011; Kan et al., 2010). These efforts have resulted in conflicting reports of the number of mutations present in a given ovarian tumor with one study reporting an average of about 3 mutations and another reporting approximately 61 mutations per tumor cancer (Cancer Genome Atlas Research, 2011; Kan et al., 2010). These studies, however, used different methods of sequencing to identify mutations and different numbers of tumor samples, with one study exclusively considering serous adenocarcinomas (Cancer Genome Atlas Research, 2011).

The Cancer Genome Atlas (TCGA) project has sought to sequence over 400 tumors to better understand what, if any, mutations are present in a majority of serous ovarian cancers. This project found a similar mutational landscape as a previous study where the majority of mutations appeared in a very small percentage of tumors (Cancer Genome Atlas Research, 2011; Kan et al., 2010). The exception to this observation appears to be TP53, which is mutated in up to 96% of cases of serous ovarian adenocarcinoma (Ahmed et al., 2010; Cancer Genome Atlas Research, 2011). A previous study found TP53 mutations in approximately 55% of ovarian tumors of all histotypes (Kan et al., 2010). The next most commonly seen mutations in serous ovarian cancer were in BRCA1 and BRCA2. These genes can harbor either germline mutations (8-9% of tumors for each locus) or, less commonly, somatic mutations (about 3% of tumors) (Cancer Genome Atlas Research, 2011; Lancaster et al., 1996; Rubin et al., 1998). After these genes, the frequency of significantly mutated genes quickly decreases to 3-6%, with different studies identifying different mutations (Cancer Genome Atlas Research, 2011; Kan et al., 2010). NF1, a negative regulator of RAS signaling, was identified as significantly mutated in ovarian tumors by both studies. These studies have also identified RB1, FAT3, CSMD3, GABRA6,

CDK12, KRAS, BRAF, AR, CTNNB1, ITPR3, CBLC, EPHB1, FRAP1, KREMEN1, MAS1L, PKHD1, and PTK7 as loci with significant low frequency mutation. These studies point to a diverse landscape of mutations existing among ovarian tumors. Because of this diverse landscape, new ideas about the pathogenesis of ovarian cancer are emerging.

In addition to a broad mutational landscape, investigations of ovarian tumors have revealed large-scale alterations at the level of somatic copy number alterations (SCNAs). Indeed, many of the SCNAs identified occur with greater frequency than most mutations. TCGA data has identified 5 copy number gains and 18 copy number losses present in over 50% of tumors studied (Cancer Genome Atlas Research, 2011). Additionally, this study identified genes associated with focal amplification including CCNE1, MYC, MECOM, TERT, and PAX8. Furthermore, depletion of PAX8 via siRNA has been reported to be lethal to ovarian cancers overexpressing this gene (Cheung et al., 2011). PTEN, RB1, and NF1 were among genes found to have deletions at a small but significant frequency (Cancer Genome Atlas Research, 2011). Other studies have also identified similar copy number losses and gains (Etemadmoghadam et al., 2009). The frequency of SCNAs observed in ovarian tumors has led to an emerging idea of genomic instability and disarray driving the evolution of this disease. Indeed, one study found that the homologous recombination pathway was altered in approximately half of ovarian tumors studied (Kan et al., 2010). This lack of DNA repair pathways could be driving the large number of SCNAs seen in ovarian tumors. The combination of defective DNA repair pathways, chromosomal instability, and frequent TP53 mutations has been postulated to be the initiating event for epithelial ovarian cancer (Bowtell, 2010).

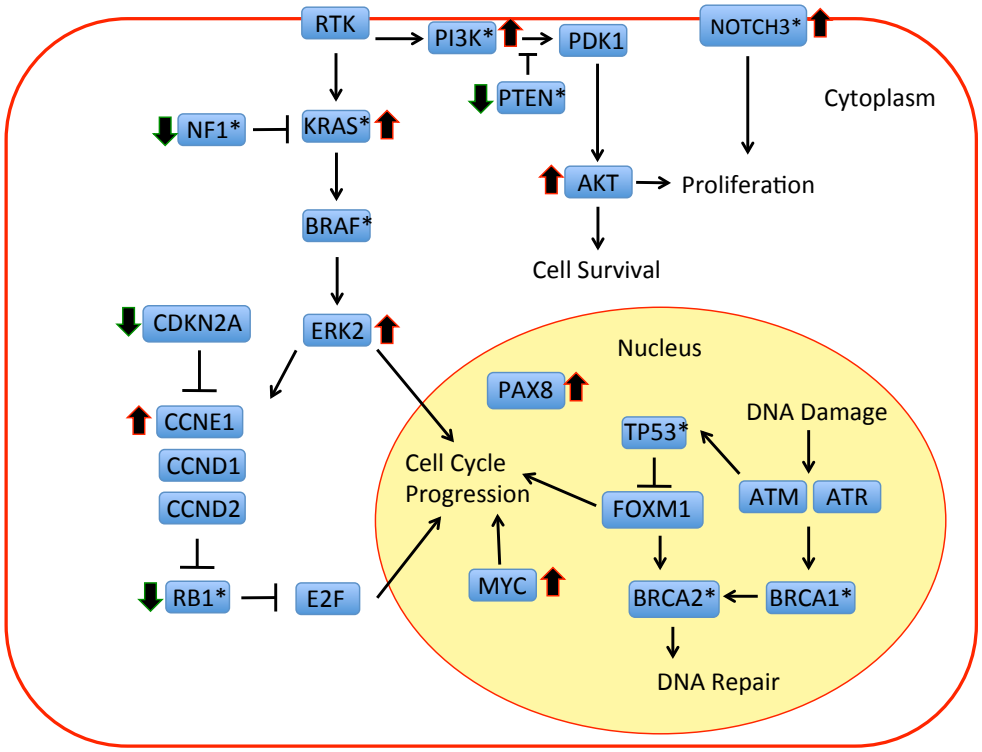

Figure 1.3. Frequently altered pathways in ovarian cancer. Arrows represent frequent copy number alterations and * denotes genes found to be mutated.

In addition to curating the spectrum of mutations and SCNAs present in ovarian cancer, attempts have been made to identify those pathways that are altered in a significant number of tumors. As previously mentioned, studies have identified homologous recombination as one process frequently altered in ovarian cancer (Kan et al., 2010). Perhaps the most frequently observed altered pathways are the PI3K and RAS signaling pathways. Multiple studies have identified these pathways as being altered in about half of ovarian tumors (Figure 3) (Cancer Genome Atlas Research, 2011; Kan et al., 2010). Multiple components of these pathways have

been observed to be mutated (NF1, PIK3CA, KRAS, BRAF), amplified (PIK3CA, KRAS, AKT1, AKT3), and deleted (PTEN, NF1) (Bast et al., 2009; Cancer Genome Atlas Research, 2011; Kan et al., 2010; Varras et al., 1999). Additional pathways have also been observed to be frequently altered in ovarian cancer, including the RB1 pathway, Notch signaling, signaling by the transcription factor FOXM1, IL6 signaling, NFκB signaling, and G-protein coupled receptor signaling (Figure 1.3) (Bast et al., 2009; Cancer Genome Atlas Research, 2011; Kan et al., 2010; Rosen et al., 2006; Wang et al., 2006). The prevalence of alterations in known cancer related pathways suggests a possibility for targeted therapy in ovarian cancer. However, therapy will most likely have to target signaling through multiple pathways to prevent resistance from arising. Molecules, such as miRNAs, that are capable of targeting multiple pathways and multiple nodes within a pathway might prove effective in uncovering novel, treatable pressure points in ovarian cancer.

1.4 miRNA Biogenesis and Function

microRNAs are small, non-coding RNAs that exert post-transcriptional control over gene expression. A mature miRNA is 18-22 nucleotides long and is generated after multiple processing steps (Figure 1.4). A long primary miRNA (pri-miRNA) is transcribed via RNA Polymerase II or III; it then folds into stem-loop hairpin secondary structures (Chen et al., 2004; Johnson et al., 2003; Johnston and Hobert, 2003; Lee et al., 2002). This pri-miRNA can contain one or multiple miRNAs (Lagos-Quintana et al., 2001; Lau et al., 2001). These hairpin structures are then processed out of the pri-miRNA transcript by the enzymes Drosha and

DGCR8 to produce a pre-miRNA of about 60-80 nucleotides in length (Lee et al., 2003; Lee et al., 2002). pre-miRNAs are then exported from the nucleus to the cytoplasm via Exportin 5 (Lund et al., 2004; Yi et al., 2003). In the cytoplasm, the enzyme Dicer further processes the pre-miRNA into a mature miRNA of 18 to 22 nucleotides (Grishok et al., 2001; Hutvagner et al., 2001; Ketting et al., 2001). After processing by Dicer, one strand of the mature miRNA is loaded onto the Argonaute (Ago) protein, which then assembles with other proteins into an RNA-induced silencing complex (RISC) (Hutvagner and Zamore, 2002; Mourelatos et al., 2002). The strand not loaded into the RISC is rapidly degraded.

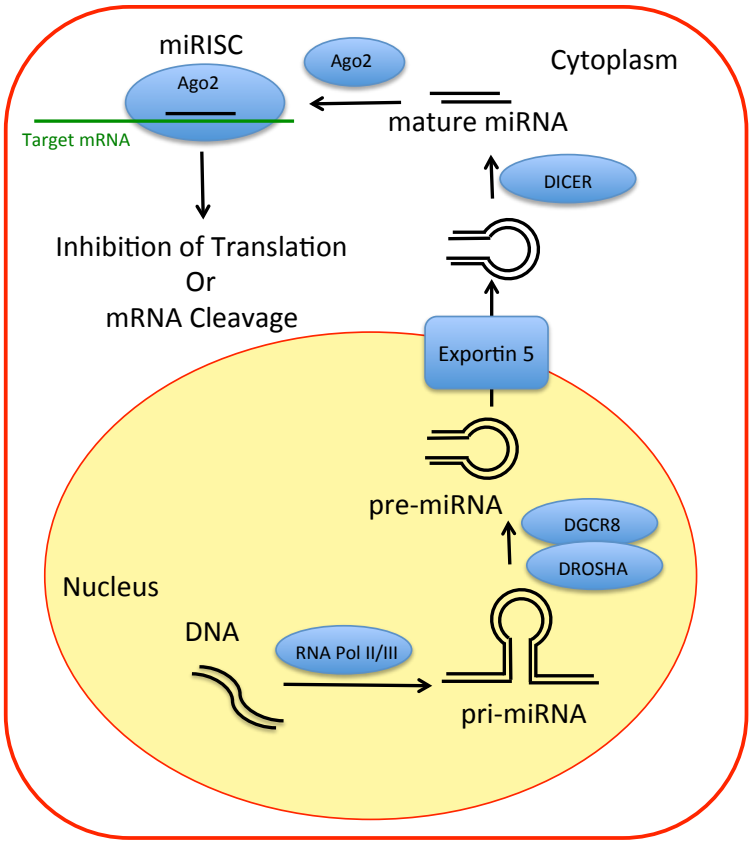

Figure 1.4. miRNA biogenesis involves multiple processing steps.

Once loaded into the RISC, the miRNA can direct modulation of target gene expression via Watson-Crick base pairing of the miRNA with a cognate target gene's 3'-untranslated region (3'-UTR). Unlike short interfering RNAs (siRNAs), miRNAs do not utilize perfect base-pairing with their targets. Binding of the miRNA-loaded RISC can either repress translation, or extensive base-pairing can lead to cleavage and decay of the target transcript (Hutvagner and Zamore, 2002; Zeng et al., 2003). While miRNAs were originally believed to effect control of gene levels mainly through inhibition of translation, recent data suggests that these small non-coding RNAs function mainly through decreased levels of target transcripts (Lim et al., 2005). Target recognition is believed to be driven by nucleotides 2-8 of the mature miRNA, termed the "seed region" of the miRNA. Base pairing between the seed region and the 3'-UTR of the target transcript defines the majority of targets for a given miRNA (Bartel, 2009; Lewis et al., 2005; Lewis et al., 2003). miRNAs exhibit what has been termed a "many-to-many" relationship with their target genes. That is to say a single miRNA can target many genes, and a single gene can be targeted by many miRNAs.

Because each miRNA can regulate many genes, they are uniquely positioned to act as rheostats of cell signaling pathways. By fine-tuning the expression of multiple genes in a signaling pathway or cell biological process, a miRNA can profoundly regulate outputs of these processes and pathways. Indeed, recent research has found that miRNAs target multiple nodes in signaling pathways such as the AKT signaling pathway (Small et al., 2010). Furthermore, recent studies have shown that overexpression of single miRNAs can reprogram fibroblasts to adopt

either cardiac or neuronal fates, again providing evidence that miRNAs can profoundly influence cell fate decisions (Nam et al., 2013; Small et al., 2010; Xue et al., 2013).

1.5 miRNAs and Ovarian Cancer

Given their ability to regulate multiple signaling pathways and cellular processes, miRNAs have somewhat unsurprisingly been implicated in multiple steps of cancer progression. However, their role as tumor suppressors or oncogenes remains unclear and confusing. Speaking to a possible tumor suppressive role, miRNAs have been found to be generally under-expressed in cancer versus normal tissue (Lu et al., 2005). Pointing to the selective pressure miRNAs can apply to emerging cancer cells, the 3'-UTRs of mRNAs of cancer cells have been found to be shorter than the same 3'-UTRs in non-cancerous cells (Mayr and Bartel, 2009). By shortening their 3'-UTRs via alternative polyadenylation sites, the cancer cells remove target sites for miRNAs and the ability of miRNAs to alter gene expression. The enzymes Dicer and Drosha, both important in biogenesis of miRNAs, have both been found to have decreased expression in over half of ovarian cancer tumors (Merritt et al., 2008). Moreover, decreased expression of Dicer correlates with decreased survival in ovarian cancer, and high expression of both Dicer and Drosha correlates with an increased median survival time of almost ten years (Merritt et al., 2008).

Although a convincing mouse model of ovarian cancer has yet to be established, work on generating such a model has shown that mice with deletions in both PTEN and DICER1 generate spontaneous ovarian tumors (Kim et al., 2012). The source of these tumors appears to the

fallopian tubes. DICER1 has also been shown to be a haploinsufficient tumor suppressor in the background of mutant RAS. Deletion of one copy of DICER1 results in greater tumor burden and faster mortality in mice with constitutively active G12D RAS conditionally expressed in their lungs (Kumar et al., 2009). Interestingly, DICER1 null mice fare better than their heterozygous littermates though still worse than wild-type mice, suggesting a possible oncogenic role for some miRNAs.

Multiple studies of miRNA expression have found significant differences in the miRNAs expressed between ovarian tumors and normal ovarian tissue. These studies have demonstrated multiple miRNAs have decreased expression in several histological subtypes of ovarian cancer with some miRNAs exhibiting subtype-specific downregulation (Dahiya et al., 2008; Iorio et al., 2007). Another study has suggested that these expression differences could be driven by copy number alterations in ovarian cancer (Zhang et al., 2008). One study looking at the dysregulation of miRNA expression in both cell lines and tumors found about half of miRNAs with aberrant expression in cell lines have similar aberrations in expression in tumors (Dahiya et al., 2008). Additionally, the miR-200 family of miRNAs (consisting of miRs-200a, -200b, -200c, -141, and -429) has been implicated in inhibiting cancer cell metastasis. These miRNAs act by targeting the transcription factors ZEB1 and ZEB2, which act to inhibit expression of E-cadherin and promote cell invasion (Gregory et al., 2008; Korpal et al., 2008; Park et al., 2008). There is evidence supporting the idea that expression of these miRNAs is lost in cancer due promoter hypermethylation (Davalos et al., 2012; Tryndyak et al., 2010; Wiklund et al., 2011).

The sum of these data suggests that miRNAs might play an important role in preventing the formation and progression of ovarian cancer.

However, miRNAs have also been implicated in oncogenesis. miRNAs such as miR-155 and miR-21 have been shown to be overexpressed in multiple cancer types, with miR-21 being shown to be upregulated in metastatic ovarian tumors relative to primary tumors (Calin et al., 2004; Eis et al., 2005; Landgraf et al., 2007; Volinia et al., 2006). Displaying the oncogenic potential of these miRNAs, transgenic mice overexpressing miR-155 develop a B-cell lymphoma, while mice overexpressing miR-21 displayed a potentiated phenotype for mutant KRAS-induced lung tumors (Costinean et al., 2006; Hatley et al., 2010). A study of patients observed that higher expression of three miRNAs (miR-410, miR-337, and miR-645) is associated with a worse prognosis in ovarian cancer patients (Shih et al., 2011). Studies have also uncovered miRNAs expressed at higher levels in ovarian tumors than normal ovarian tissue, with the miR-200 family being some of the most highly overexpressed miRNAs in ovarian cancer (Iorio et al., 2007). However, more investigation needs to be conducted to conclusively determine the role of the miR-200 family in ovarian cancer as other studies have shown that this miRNA might not be overexpressed in ovarian tumors (Dahiya et al., 2008). Further confusing this miRNA family's role, overexpression of miR-141, a member of the miR-200 family, has been shown to induce resistance to platinum therapy in ovarian cancer cell lines; whereas overexpression of miR-200c has been shown to drive sensitivity to taxane therapy (Cittelly et al., 2012; Holleman et al., 2011; van Jaarsveld et al., 2012). Thus more investigation is required to determine the exact role the miR-200 family plays in cancer progression. Other miRNAs have

also been implicated in modulating drug sensitivity. miR-135a has been to shown have increased expression in taxane-resistant ovarian cancer and non-small cell lung cancer cells, with reduction of this miRNA restoring taxane sensitivity (Holleman et al., 2011).

In reality, the impact of changes in miRNA expression is likely to be context specific. As an example, miR-146a has been shown to target IRAK1 and TRAF6 to prevent activation of the NFκB pathway, thus exerting a tumor suppressive effect (Taganov et al., 2006). However, miR-146a can also reduce levels of BRCA1, thus acting in an oncogenic manner (Garcia et al., 2011a). Consistent with the context sensitivity of miR-146a's actions, there have been reports that miR-146a is upregulated in metastatic ovarian tumors relative to matched primary samples, possibly driving resistance to platinum therapy (Vang et al., 2013). Other reports have demonstrated miR-146a overexpression leads to apoptosis of non-small cell lung cancer cells (Chen et al., 2013). A polymorphism in the gene encoding miR-146a has been identified in multiple melanoma cell lines with more aggressive growth characteristics, and this polymorphism is enriched in patients with melanomas versus control patients, again suggesting a role in cancer progression for this miRNA(Yamashita et al., 2013). However, the functional impact of this polymorphism has yet to be shown. Pilot studies suggested that this polymorphism might correlate with early onset of ovarian cancer, but a larger study has failed to confirm this correlation (Garcia et al., 2011b; Pastrello et al., 2010; Shen et al., 2008). Suggesting a tumor suppressive role for this miRNA, knockout mice of miR-146a have been reported to form both lymphomas and sarcomas (Zhao et al., 2011). Therefore, the context of activation of miR-146a appears to be important in the net role the miRNA plays in tumor

formation. More likely, most miRNAs display similar context sensitivity, where the cellular environment of their expression or loss determines the net effect on the cell and cancer progression.

The urgent need for new therapies in ovarian cancer has driven large-scale studies to elucidate linchpin biology underlying this disease in the hopes of discovering vulnerabilities. miRNAs not only play an invaluable role interrogating the biology of ovarian cancer in the lab, but they may also become an important treatment option for diseases such as EOC in the clinic.

CHAPTER TWO
MAPPING THE LANDSCAPE OF ACQUIRED VULNERABILITIES IN OVARIAN CANCER

2.1 Introduction

Epithelial ovarian cancer (EOC) is the most lethal gynecologic malignancy in the United States (Siegel et al., 2012). EOC is considered disproportionately lethal in that it is the 9th most common cancer in women but responsible for the 5th most deaths (Siegel et al., 2012). Patients diagnosed with this disease have a poor overall 5-year survival, which is driven by a combination of late diagnosis in the vast majority of cases (over 60% of patients are diagnosed after metastasis of the disease) and the broad appearance of resistance to current platinum-taxane chemotherapy. Recent advances in treatment of this disease have been limited to empirical optimization of chemotherapeutic agents and improved delivery of drugs (Armstrong et al., 2006). Given that these advances have only yielded small improvements in overall survival of ovarian cancer patients, there is an urgent need for novel treatment modalities. A greater understanding of the linchpin biology of this disease will provide inroads toward the development of new therapies.

Multiple studies, including work by The Cancer Genome Atlas (TCGA), have conducted a large-scale effort to annotate the landscape of genetic alterations associated with this disease. These studies only identified p53 mutations as prevalent in a majority of tumors, while all other somatic mutations occur with much less frequency, representing a flat mutational landscape (Cancer Genome Atlas Research, 2011; Kan et al., 2010). In contrast the broad diversity of

mutations, frequent copy number alterations have been identified (Cancer Genome Atlas Research, 2011; Etemadmoghadam et al., 2009). This vast genetic diversity and frequent chromosomal aberrations have given rise to the idea that ovarian tumors are driven by a "turbulent genome."

Finding drug targets within this genetic cacophony has proven to be an enormous challenge. Recent studies have implicated miRNAs as possible tumor suppressors in this disease suggesting these molecules as possible starting point in the search for new interventions. Dicer, an RNase involved in miRNA processing, has been reported to be a haploinsufficient tumor suppressor in mice, and deletion of Dicer and PTEN in mice is sufficient to result in spontaneous formation of ovarian tumors (Kim et al., 2012; Kumar et al., 2009). Furthermore, Dicer and Drosha, another miRNA processing enzyme, show decreased expression in over half of ovarian tumors sampled, and expression of Dicer correlates with patient survival (Merritt et al., 2008). Finally, the 3'-untranslated regions (3'-UTRs) of mRNAs have been shown to be shortened in cancer cells, releasing oncogenes from miRNA regulation (Mayr and Bartel, 2009). All of these reports suggest that deregulation of miRNA expression might be an important common element in ovarian cancer progression.

To harness the commonality of miRNA deregulation, we conducted a broad gain-of-function miRNA mimic cell viability screen in multiple ovarian cancer cell lines to survey the landscape of vulnerabilities in ovarian cancer. We conducted this screen to investigate if a "turbulent genome" gave rise to multiple idiosyncratic acquired vulnerabilities or if these genetic

changes collapsed down to a few common vulnerabilities. To our knowledge this is the first broad-scale gain-of-function miRNA mimic to attempt to map vulnerabilities in ovarian cancer. A miRNA-based approach possessed the added benefit of being able to assay a maximal amount of gene space with minimal experiments. Also, the ability of multi-genic nature of miRNA perturbations might bypass some of the shortcomings of single gene lethality screens such as: functional redundancy of genes supporting key biological processes, lack of effective siRNAs representing every gene in a library, and continued, efficient function of some genes despite siRNA-mediated knockdown. However, this approach was contingent on the ability to decipher which miRNA targets were functionally relevant to a cell viability phenotype.

The screen revealed that 108 miRNA mimics reduced cell viability in at least 1 of 16 cell lines screened. These miRNAs displayed a strikingly idiosyncratic pattern of toxicity throughout the panel with the majority of mimics reducing viability in only 1 or 2 cell lines. Analysis of two miRNAs with idiosyncratic activity across the panel revealed the ability of computationally predicted targets to accurately predict physiologic effects of miRNA mimic expression, supporting our approach. Two miRNAs with broad activity in the cell line panel screened were found to regulate novel targets supporting ovarian cancer cell survival. Both of these miRNAs appeared to drive cell differentiation programs speaking to the possible commonality of loss of miRNA regulation is a necessary step for ovarian cancer cell to deflect cellular differentiation. The penetrant phenotype observed in this panel of cell lines suggested that re-engagement of these differentiation programs had catastrophic consequences in ovarian cancer cells.

2.2 Results

2.2.1 A miRNA Screen of Ovarian Cancer Cell Lines Revealed Multiple Idiosyncratic Vulnerabilities

This screen was conducted similarly to previously published screens, but here we utilized a 417 miRNA mimic library consisting of the intersection of two Dharmacon miRIDIAN mimic libraries containing mimics of all annotated human miRNAs in miRBase 8 and miRBase 10.1 (Ganesan et al., 2008; Whitehurst et al., 2007). To capture some of the diversity of genetic alterations seen in patients, we utilized a panel of 16 ovarian cancer cell lines. This panel included 11 traditionally used ovarian cancer cell lines and 3 cell lines (HCC5012, HCC5019, HCC5030) recently derived from malignant peritoneal effusions of patients with high-grade serous papillary adenocarcinoma of the ovary. Being non-clonal and having been cultured only a short period of time, these recently derived cell lines should more faithfully capture the genetic heterogeneity within ovarian tumors. Thus, these cell lines may more closely model the disease than traditional, clonal cell lines. A pair of cell lines (PEO1 and PEO4) derived from a single patient was also included in order to further capture the diversity within a single patient's tumor.

Our screen identified 108 mimics, representing 94 unique miRNAs, that reduced cell viability (z-score $\leq$ -2) in at least one cell line screened. In order to better view the patterns of reduced viability, we subjected hits to two-way unsupervised hierarchical clustering using Euclidian distance of their z-scores (Figure 2.1A). This cluster revealed that the majority of screen hits were idiosyncratic, reducing viability in only one or two cell lines. We then

investigated the nature of miRNAs that clustered near to each other. Manual curation of the seed sequence associated with each miRNA mimic revealed a tendency for mimics with the same seed to cluster together, suggesting that the decreased cell viability observed is dependent on miRNA seed sequence. Confirming the idiosyncratic nature of most hits, a histogram displaying hit penetrance via the number of non-redundant hits in a given number of cell lines revealed that only 20% of hits were penetrant in 3 or more lines and no mimic reduced viability in more than 9 cell lines (Figure 2.1B). Because idiosyncratic hits might simply represent artifacts of cell culture, we investigated the significance of these hits. With few hits, the SKOV3 cell line was one of the most resistant lines screened (Figure A1.1). However, mining TCGA miRNA expression and outcome data, we found that two idiosyncratic SKOV3 hits correlated with patient survival. We found patients with higher expression of miR-146a have increased overall survival and an increased median overall survival time of 17.1 months (Figure 2.1C). miR-505 expression also significantly correlated with patient outcomes, having a 10.4 month increase in median overall survival in patients with higher expression of this miRNA (Figure 2.1C). Correlation with patient prognosis indicated that perhaps these idiosyncratic hits were targeting biology underlying ovarian tumors.

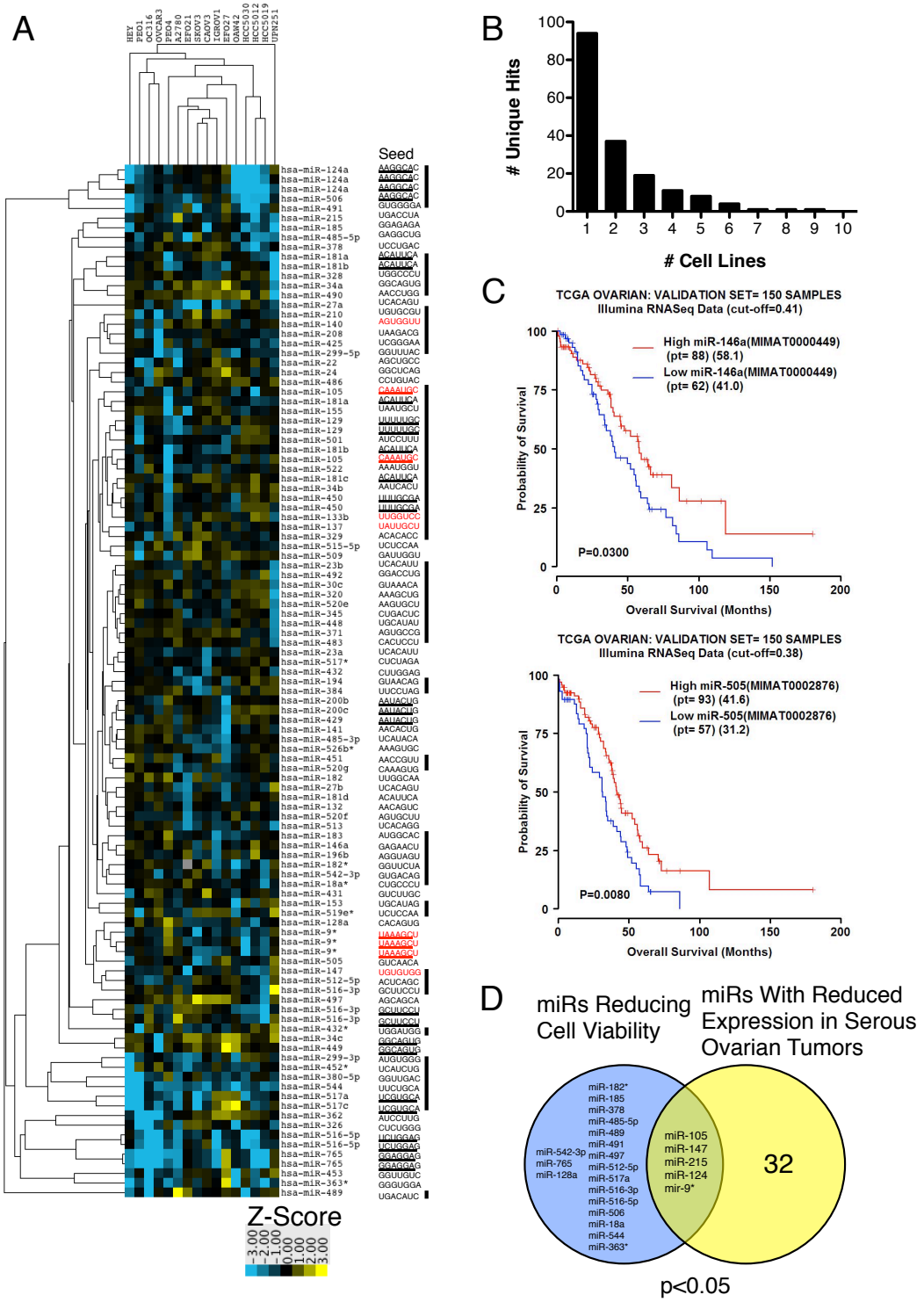
A
HEY
PEO1
OCI16
OVCAR3
PEO4
A2780
EFO21
SKOV3
CAOV3
IGROV1
EFO27
OAW42
HCC1010
HCC5012
HCC5019
UPN251
Seed
hsa-miR-124a
hsa-miR-124a
hsa-miR-124a
hsa-miR-506
hsa-miR-491
hsa-miR-215
hsa-miR-185
hsa-miR-485-5p
hsa-miR-378
hsa-miR-181a
hsa-miR-181b
hsa-miR-328
hsa-miR-34a
hsa-miR-490
hsa-miR-27a
hsa-miR-210
hsa-miR-140
hsa-miR-208
hsa-miR-425
hsa-miR-299-5p
hsa-miR-22
hsa-miR-24
hsa-miR-486
hsa-miR-105
hsa-miR-181a
hsa-miR-155
hsa-miR-129
hsa-miR-129
hsa-miR-501
hsa-miR-181b
hsa-miR-105
hsa-miR-522
hsa-miR-181c
hsa-miR-34b
hsa-miR-450
hsa-miR-450
hsa-miR-133b
hsa-miR-137
hsa-miR-329
hsa-miR-515-5p
hsa-miR-509
hsa-miR-23b
hsa-miR-492
hsa-miR-30c
hsa-miR-320
hsa-miR-520e
hsa-miR-345
hsa-miR-448
hsa-miR-371
hsa-miR-483
hsa-miR-23a
hsa-miR-517*
hsa-miR-432
hsa-miR-194
hsa-miR-384
hsa-miR-200b
hsa-miR-200c
hsa-miR-429
hsa-miR-141
hsa-miR-485-3p
hsa-miR-526b*
hsa-miR-451
hsa-miR-520g
hsa-miR-182
hsa-miR-27b
hsa-miR-181d
hsa-miR-132
hsa-miR-520f
hsa-miR-513
hsa-miR-183
hsa-miR-146a
hsa-miR-196b
hsa-miR-182*
hsa-miR-542-3p
hsa-miR-18a*
hsa-miR-431
hsa-miR-153
hsa-miR-519e*
hsa-miR-128a
hsa-miR-9*
hsa-miR-9*
hsa-miR-9*
hsa-miR-505
hsa-miR-147
hsa-miR-512-5p
hsa-miR-516-3p
hsa-miR-497
hsa-miR-516-3p
hsa-miR-516-3p
hsa-miR-432*
hsa-miR-34c
hsa-miR-449
hsa-miR-299-3p
hsa-miR-452*
hsa-miR-380-5p
hsa-miR-544
hsa-miR-517a
hsa-miR-517c
hsa-miR-362
hsa-miR-326
hsa-miR-516-5p
hsa-miR-516-5p
hsa-miR-765
hsa-miR-765
hsa-miR-453
hsa-miR-363*
hsa-miR-489
Z-Score
-3.00
-2.00
-1.00
0.00
1.00
2.00
3.00
B
Unique Hits
Cell Lines
C
TCGA OVARIAN: VALIDATION SET= 150 SAMPLES
Illumina RNASeq Data (cut-off=0.41)
High miR-146a(MIMAT0000449)
(pt= 88) (58.1)
Low miR-146a(MIMAT0000449)
(pt= 62) (41.0)
Probability of Survival
P=0.0300
Overall Survival (Months)
TCGA OVARIAN: VALIDATION SET= 150 SAMPLES
Illumina RNASeq Data (cut-off=0.38)
High miR-505(MIMAT0002876)
(pt= 93) (41.6)
Low miR-505(MIMAT0002876)
(pt= 57) (31.2)
Probability of Survival
P=0.0080
Overall Survival (Months)
D
miRs Reducing
Cell Viability
miRs With Reduced
Expression in Serous
Ovarian Tumors
miR-182*
miR-185
miR-378
miR-485-5p
miR-489
miR-491
miR-497
miR-512-5p
miR-517a
miR-516-3p
miR-516-5p
miR-506
miR-18a
miR-544
miR-363*
miR-542-3p
miR-765
miR-128a
miR-105
miR-147
miR-215
miR-124
mir-9*
32
p<0.05

Figure 2.1. The landscape of vulnerabilities in ovarian cancer is highly idiosyncratic.

(**A)** A two-way hierarchical cluster using Euclidian distance of z-scores showed most screen hits were idiosyncratic and that the panel of cell lines shared few common vulnerabilities. This cluster contained any miRNA mimic with a z-score ≤ -2 in at least one cell line screened. Seed sequences of each miRNA mimic are provided to the right. Bars to the right of seeds represent cluster boundaries. Seeds represented more than once in each cluster are underlined. Seeds in red have been reported to have decreased expression in serous, clear cell, and endometrioid ovarian cancer relative to normal tissue (Iorio et al., 2007).

(B) A histogram showing the number of non-redundant hits binned by number of cell lines revealed most hits are penetrant in only 1 or 2 cell lines with none penetrant in more than 9.

(C) Expression of miRNAs miR-146a and miR-505 correlated with overall survival in ovarian cancer patients. Displayed is the validation set (n=150 samples) of Illumina miRseq data, for training set data and Agilent data see Figure S1.

(D) Hits in non-clonal, short culture cell lines HCC5012, HCC5019, and HCC5030 were enriched for miRNAs with reduced expression in serous ovarian cancer (Iorio et al., 2007). p-value derived from hypergeometric distribution.

To further investigate the relevance of hits from this screen, we asked if those miRNAs toxic in the non-clonal short-term culture cell lines, which should most closely resemble tumors, could be relevant in human disease. Hits in these lines were significantly enriched for miRNAs with reduced expression in serous ovarian tumors (Iorio et al., 2007) (Figure 2.1D). This data continued to suggest idiosyncratic hits could be relevant to the biology of ovarian tumors in patients and not simply represent artifacts of cell culture. Therefore, we wondered whether they might exploit unique vulnerabilities.

2.2.2 Idiosyncratic Hits Represent Specific Vulnerabilities

To explore the nature of idiosyncratic hits, we utilized mimics with differential toxicity between the PEO1 and PEO4 cell lines. These lines are derived from the same patient, which should minimize the differences that might define sensitivity. Cytogenetic analyses have shown that these two cell lines descended from a common ancestor as opposed to one arising from direct linear descent (Cooke et al., 2010; Wolf et al., 1987). Derived later in the patient's treatment, the PEO4 cell line is a model for recurrent, platinum-resistant EOC (Figure A1.2). A scatter plot of the z-scores of each mimic from the PEO1 and PEO4 screens revealed two distinct tails of hits (Figure 2.2A). Very few mimics had z-scores < -2 in both screens suggesting possible fundamental differences in biology between these two cell lines. In order to determine if endogenous miRNA expression influenced the phenotype observed in the screens, we conducted a miRNA expression array for PEO1, PEO4, and human ovarian surface epithelium

(HOSE) cells (Figure 2.2B). These arrays revealed multiple miRNAs with altered expression in PEO1 and PEO4 cells relative to HOSE cells and showed different global miRNA expression patterns in PEO1 and PEO4 cells.

Using a scatter plot of each miRNA's endogenous expression in PEO1 and PEO4 cells, we found that the phenotype of a mimic was unrelated to endogenous expression of its respective miRNA (Figure 2.2C). A plot of the expression of each miRNA relative to HOSE cells revealed that hits in each cell line were not driven by gain or loss of endogenous expression of their respective miRNAs (Figure 2.2C). These results suggested that specificity of mimic toxicity was not defined by expression of the endogenous miRNA. To verify that dosage effects were not driving specificity, we performed dosage response curves with the PEO1-specific hit miR-210 in both lines. We observed that even at a 10-fold decrease in dosage PEO1 was still extremely sensitive to this miRNA, while increasing the dosage 4-fold in PEO4 cells did sensitize this resistant cell line (Figure A1.2). These observations supported the idea that differential toxicity of mimics was characterized by different acquired vulnerabilities in PEO1 and PEO4 cells.

In order to determine if the genetic background of a cell line specified sensitivity to a mimic, we performed whole exome and RNA sequencing on both of these lines. Because we did not have a matched normal cell line for the PEO1 and PEO4 cell lines, we filtered single nucleotide variation (SNV) data through 16 normal human exomes that had been selected as controls for an unrelated study to remove common polymorphisms. In addition to using exome sequencing data to capture SNV data, we obtained copy number variation (CNV) data for these

two cell lines by using their read depth at each locus relative to a non-tumorigenic reference cell line. SNV data revealed multiple SNVs shared by PEO1 and PEO4 cell lines, representing either germ line mutations or somatic mutations acquired before divergence from the nearest common ancestor. Each cell line also had many unique SNVs, highlighting the differences between these two lines (Figure 2.2D). The CNV data showed similar results to the SNV data with both lines displaying unique copy number alterations, though they also shared many alterations. Finally, RNA sequencing revealed differences in the transcriptomes of these two cell lines, which once again highlighted the differences between PEO1 and PEO4 cells (Figure 2.2D).

We then leveraged this high-resolution data to interrogate the biology underlying PEO4-specific hits. miR-155 and miR-181b were found to reduce cell viability specifically in PEO4 cells and did not decrease cell viability in either immortalized human hepatocytes (IHH) or HOSE cells (Figure 2.3A). Pointing to a role for miR-155 in ovarian tumors, expression of this miRNA is decreased in both ovarian tumors and ovarian cancer cell lines relative to normal tissues and cell lines respectively (Dahiya et al., 2008; Zhang et al., 2008). Because seed sequences clustered near each other, suggesting their importance to the observed viability phenotype, we inquired if these two miRNAs (with similar phenotypes but different seed sequences) targeted genes converging on similar cellular processes. Using two computational tools, miRPath V1.0 and miRSystem, which query whether seed-predicted targets of a given miRNA or group of miRNAs are enriched for a particular gene set, we found that the predicted targets of miR-155 and miR-181b were enriched for two signaling pathways: signaling

downstream of the insulin receptor and TGFβ signaling pathway (Lu et al., 2012; Papadopoulos et al., 2009). Analysis of the predicted targets of miR-155 and miR-181b in TargetScan (Lewis et al., 2003) uncovered multiple nodes of the AKT and MAPK signaling pathways, both of which are downstream of the insulin receptor (Figure A1.3). Examination of the high-resolution genomic data acquired from the PEO1 and PEO4 lines revealed alterations in both of these pathways (Figure A1.3). PEO1 cells possessed a truncation mutation in the RAS GTPase activating protein (GAP) NF1, which removed the functional domain of this protein. Also, PEO4 cells had an amplification in the AKT pathway inhibitor PTEN. Empirical examination of signaling through the AKT pathway in response to serum stimulation after serum deprivation overnight revealed decreased AKT phosphorylation and activation in PEO4 cells relative to PEO1 cells consistent with overexpression of PTEN (Figure 2.3B).

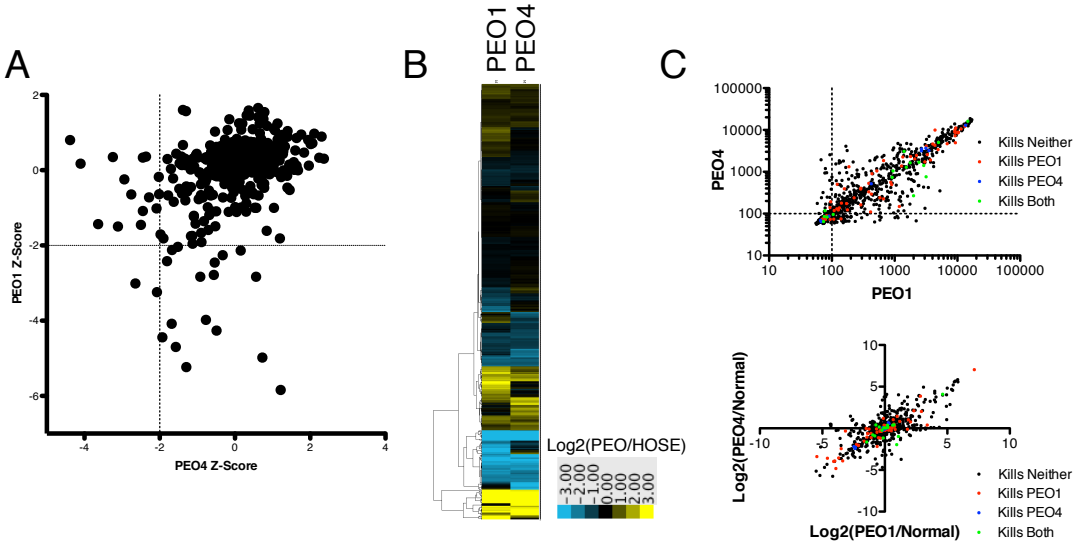
A
PEO1 Z-Score
PEO4 Z-Score
B
PEO1
PEO4
Log2(PEO/HOSE)
C
PEO4
PEO1
Kills Neither
Kills PEO1
Kills PEO4
Kills Both
Log2(PEO4/Normal)
Log2(PEO1/Normal)

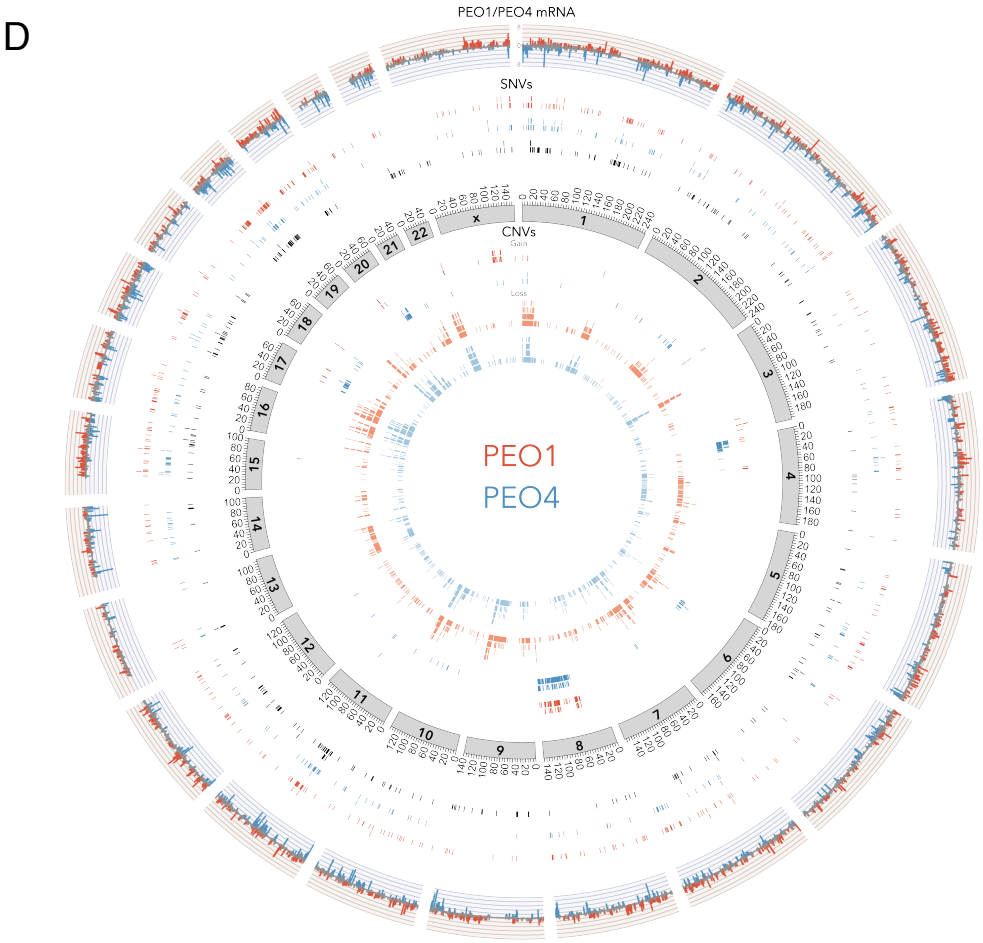
D
PEO1/PEO4 mRNA
SNVs
CNVs
Gain
Loss
PEO1
PEO4

Figure 2.2. Idiosyncratic hits represent specific vulnerabilities and are not expression driven.

(A) A scatter plot of Z-scores of screens of PEO1 and PEO4 cells displayed two tails of specific hits and very few common hits.

(B) A unidirectional cluster using the Euclidian distance of the $\log_2$ of the ratio of miRNA expression in PEO1 or PEO4 cells and HOSE cells revealed different global miRNA expression patterns.

(**C)** A scatter plot of the expression values of each miRNA in PEO1 and PEO4 showed that screen hits are not enriched for miRNAs of any expression level. Furthermore, a scatter plot of the $\log_2$ of the ratio of expression in PEO1 or PEO4 and HOSE cells did not reveal enrichment of specific hits for miRNAs with reduced relative expression.

(D) A circos plot of high-resolution genomic data of PEO1 and PEO4 cell lines displayed many genomic differences between PEO1 and PEO4 cells. The outer track displays relative expression of genes (the $\log_2$ of the ratio of (RPKM+1) values of PEO1 to PEO4). Peaks in red show genes with greater than 2-fold overexpression in PEO1 cells, peaks in blue greater than 2-fold overexpression in PEO4 cells, and peaks in grey represent genes without a 2-fold expression difference. The next three inner tracks represent SNV data, with SNVs unique to PEO1 in red, PEO4 in blue, and common SNVs in black. The next inner track is an axis representing chromosome position. The inner four tracks display CNV data with the outer two tracks displaying copy number gains (defined by a read depth ratio of ≥ 1.5 when compared to the

reference cell line) with PEO1 in red and PEO4 in blue. The inside two tracks represent copy number losses (read depth ratio ≤ 0.5) with PEO1 in light red and PEO4 in light blue.

A similar experiment was performed in PEO1 cells transfected with either mimic negative control, miR-155, or miR-181b 48 hours after transfection. Expression of miR-155 and miR-181b abrogated AKT activation as seen through decreased levels of phosphorylation at T308 by both mimics and decreased phosphorylation at S473 by miR-155 (the only mimic predicted to target this phosphorylation site) in response to serum stimulation (Figure 2.3C). However, direct pharmacologic inhibition of AKT signaling using either a PI3K or an AKT inhibitor failed to recapitulate the specificity of mimic expression (Figure 2.3D). In fact, PEO1 cells were more sensitive to siRNA-mediated knockdown of PTEN, AKT1, and AKT2 as might be expected given previous evidence that cell lines and tumors with alteration in the AKT pathway are addicted to it (Hanrahan et al., 2012) (Figure 2.3D). However, we were encouraged that target prediction could accurately describe effects of mimic expression, though these effects did not explain the specificity of toxicity in this case.

Because pathway analysis of the predicted targets of miR-155 and miR-181b also found enrichment in the TGFβ signaling pathway, we analyzed high resolution genomic data for a difference in signaling down this pathway similar to the AKT pathway (Figure A1.3). This analysis suggested the possibility of increased basal signal through the TGFβ pathway in PEO4 cells, as PEO1 cells expressed higher levels of the E3 ubiquitin ligase SMURF2, which promotes SMAD protein degradation. Western blots confirmed higher protein levels of SMAD2 and SMAD4 in PEO4 cells and increased activating phosphorylation of SMAD 2 and SMAD3 in response to 10 ng/mL TGFβ1 stimulation (Figure 2.3E). However, direct interrogation of the

functional consequences of decreased signaling along this pathway via siRNA-mediated knockdown of SMAD2 and SMAD3 revealed a higher dependence on TGFβ signaling in PEO1 cells (Figure 2.3F).

As both AKT and TGFβ signaling have been implicated in epithelial-to-mesenchymal transition, we investigated if there was a difference in the epithelial and mesenchymal status of these two cells lines. Immunofluorescence revealed a difference between E-cadherin staining in PEO1 and PEO4 cells (Figure 2.3G). E-cadherin was mainly membrane-localized in PEO4 cells, indicative of an epithelial phenotype. PEO1 cells exhibited punctate perinuclear staining, suggesting a more mesenchymal phenotype. 48 hours after transfection with either miR-155 or miR-181b mimic, E-cadherin staining in PEO4 appeared to be less membrane localized and more punctate, a staining pattern reminiscent of PEO1 cells (Figure 2.3G). This finding suggested that epithelial status or E-cadherin localization might define PEO4 cells' sensitivity to these miRNAs. A panel of 46 non-small cell lung cancer (NSCLC) cell lines previously screened with a separate library containing both miR-155 and miR-181a (a family member of miR-181b) showed significant correlation in viability between these two mimics (Figure 2.3H). Furthermore, a previous report has defined the epithelial and mesenchymal status of each of these NSCLC cell lines using a gene expression signature (Byers et al., 2013). 5 of the 7 lines sensitive to expression of these mimics (defined as a greater than 50% reduction in cell viability) were classified as epithelial by this signature. This further suggested that miR-155 and miR-181b might be converging on a cellular process that defines sensitivity to these miRNAs and that

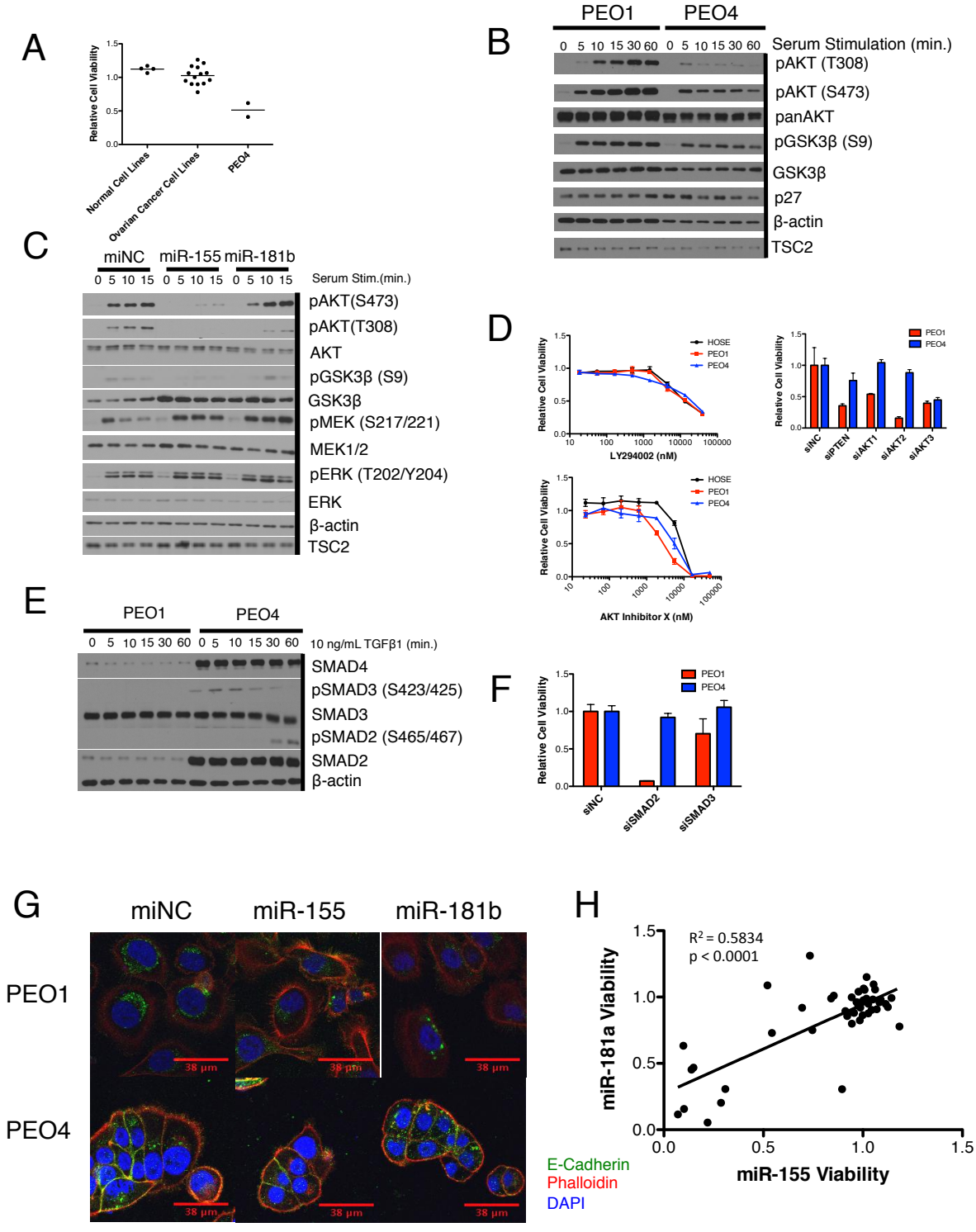
A
Relative Cell Viability
Normal Cell Lines
Ovarian Cancer Cell Lines
PEO4
B
PEO1
PEO4
0 5 10 15 30 60 0 5 10 15 30 60
Serum Stimulation (min.)
pAKT (T308)
pAKT (S473)
panAKT
pGSK3β (S9)
GSK3β
p27
β-actin
TSC2
C
miNC
miR-155
miR-181b
0 5 10 15 0 5 10 15 0 5 10 15
Serum Stim.(min.)
pAKT(S473)
pAKT(T308)
AKT
pGSK3β (S9)
GSK3β
pMEK (S217/221)
MEK1/2
pERK (T202/Y204)
ERK
β-actin
TSC2
D
HOSE
PEO1
PEO4
Relative Cell Viability
LY294002 (nM)
AKT Inhibitor X (nM)
siNC
siPTEN
siAKT1
siAKT2
siAKT3
E
PEO1
PEO4
0 5 10 15 30 60 0 5 10 15 30 60
10 ng/mL TGFβ1 (min.)
SMAD4
pSMAD3 (S423/425)
SMAD3
pSMAD2 (S465/467)
SMAD2
β-actin
F
Relative Cell Viability
siNC
siSMAD2
siSMAD3
G
miNC
miR-155
miR-181b
PEO1
PEO4
38 μm
E-Cadherin
Phalloidin
DAPI
H
R² = 0.5834
p < 0.0001
miR-181a Viability
miR-155 Viability

Figure 2.3. Target prediction of PEO4-specific miRNAs accurately described effects of mimic expression.

(A) miR-155 and miR-181b selectively reduced PEO4 cell viability across a panel of ovarian cancer lines. Each data point represents the mean of 3 experiments in a single cell line, and the lines represent the mean of all points in a column. N –IHH and HOSE; EOC – other ovarian cancer cell lines.

(B) Western blots showed decreased AKT phosphorylation at both T308 and S473 in PEO4 cells in response to serum stimulation of cells deprived of serum overnight. Decreased AKT activity was seen through decreased phosphorylation of GSK3β at S9.

(C) Western blots revealed abrogation of serum-induced AKT phosphorylation at S473 and T308 in response to expression of miR-155 mimic and decreased of T308 phosphorylation with expression of miR-181b mimic. Decreased phosphorylation of GSK3β as S9 was seen in response to both mimics.

(D) Direct inhibition of the AKT signaling pathway using either PI3K inhibitor LY294002 or AKT Inhibitor X did not reveal a differential dependence on AKT signaling between PEO1 and PEO4 cells. siRNA-mediated knockdown of PTEN, AKT1, AKT2, and AKT3, revealed decreased viability in PEO1 cells. Each point/bar represents the mean of 3 experiments ± SD.

(E) Western blots showed increased protein levels of SMAD2 and SMAD4 in PEO4 cells and increased activating phosphorylation of SMAD2 and SMAD3 in response to 10 ng/mL TGFβ1 stimulation of cells serum starved overnight.

(F) siRNA-mediated knockdown of SMAD2 and SMAD3 reduced viability in PEO1 cells. Each bar represents the mean of three experiments ± SD.

(G) E-cadherin staining revealed differences in localization between PEO1 and PEO4 cells. miR-155 and miR-181b reduced membrane-localized E-cadherin in PEO4. Cells were counterstained with Texas Red-conjugated phalloidin and DAPI.

(H) Cell viability upon expression of miR-155 and miR-181a mimics in 46 NSCLC cell lines correlated. Each data point represents the mean of 3 experiments. R^2 generated using Pearson correlation.

an epithelial status might be necessary but not sufficient to define this sensitivity. Because we had shown the ability to utilize target space to accurately predict the effects of mimic expression, we focused on two mimics with greater penetrance in the panel of cell lines to hopefully uncover novel linchpin biology supporting cancer cell survival.

2.2.3 miR-517a Targets Cell Viability and Differentiation

Normally expressed in the placenta, recent studies have suggested that anomalous expression of miR-517a in somatic tissue via demethylating agents can act in a tumor suppressive manner (Morales-Prieto et al., 2012; Yoshitomi et al., 2011). miR-517a greatly reduced viability in multiple EOC cell lines while not reducing viability in two normal cell lines (IHH and HOSE) (Figure 2.4A). Additionally, 46 NSCLC cell lines were screened with a library including the miR-517a mimic and showed similar results to the EOC cell line screen, indicating miR-517a might target a cellular process important in multiple cancer settings (Figure 2.4B).

In order to determine the effects of miR-517a exposure in vivo, we adapted a previously published protocol and intraperitoneally injected SKOV3 cells in nude mice, allowing tumors to seed for seven days (Landen et al., 2005). Mice were then treated twice weekly with either mimic negative control or miR-517a incorporated into DOPC neutral liposomes for four weeks. Treatment with miR-517a greatly reduced tumor burden in mice relative to negative control, seen through significantly fewer tumor nodules and significantly less tumor burden by weight (Figure

2.4C). Thus, miR-517a displayed the ability to reduce cell viability in vivo and not just in cell culture.

To identify functionally relevant predicted targets of miR-517a, we took advantage of previously completed whole genome siRNA screens in 12 NSCLC cell lines, 4 of which were sensitive to miR-517a, and found 2 predicted targets with strong correlation to miR-517a (Figure 2.4D). We then asked if depletion of these two targets in ovarian cancer cell lines could phenocopy miR-517a expression. Knockdown of ARCN1 closely phenocopied miR-517a expression, but knockdown of USP1 significantly decreased cell viability in only PEO1 cells (Figure 2.4E). Western blots showed that expression of miR-517a mimic in two EOC cell lines reduced protein levels of ARCN1 and USP1 (Figure 2.4F). Previous reports show that USP1 deubiquitinates ID proteins, and that these ID proteins repress p21 expression to maintain a stem cell-like phenotype in osteosarcoma cells (Williams et al., 2011). Consistent with these reports, we saw a decrease in ID1 and ID2 protein levels and an induction of p21 expression upon expression of miR-517a mimic (Figure 2.4F). Interestingly, the PEO1 cells were the most sensitive to USP1 depletion and also showed a greater induction of p21 than an insensitive line. These data suggested that the ability to strongly induce p21 might define sensitivity to USP1 depletion. In EOC cell lines, ARCN1, which encodes a member of the coatamer complex, was responsible for the miR-517a phenotype observed, supporting cell viability through an as yet unelucidated mechanism. However, USP1 might be an important target of miR-517a in other

settings, such as NSCLC, and might drive cell cycle progression through repression of p21 expression (Figure 2.4G).

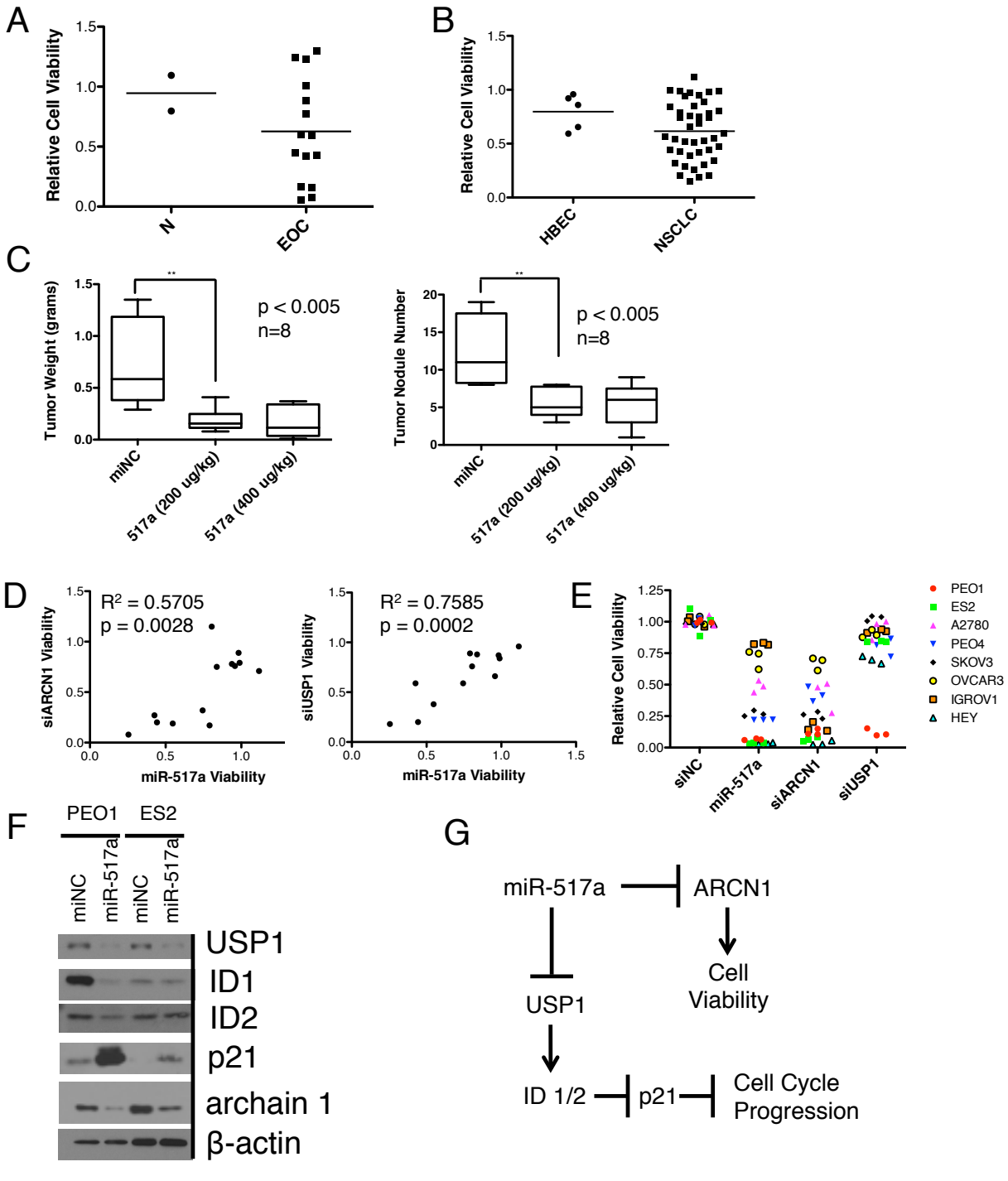
A
Relative Cell Viability
1.5
1.0
0.5
0.0
N
EOC
B
Relative Cell Viability
1.5
1.0
0.5
0.0
HBEC
NSCLC
C
Tumor Weight (grams)
1.5
1.0
0.5
0.0
**
p < 0.005
n=8
miNC
517a (200 ug/kg)
517a (400 ug/kg)
Tumor Nodule Number
20
15
10
5
0
**
p < 0.005
n=8
miNC
517a (200 ug/kg)
517a (400 ug/kg)
D
siARCN1 Viability
R2 = 0.5705
p = 0.0028
1.5
1.0
0.5
0.0
0.0
0.5
1.0
miR-517a Viability
siUSP1 Viability
R2 = 0.7585
p = 0.0002
1.5
1.0
0.5
0.0
0.0
0.5
1.0
1.5
miR-517a Viability
E
Relative Cell Viability
1.25
1.00
0.75
0.50
0.25
0.00
siNC
miR-517a
siARCN1
siUSP1
PEO1
ES2
A2780
PEO4
SKOV3
OVCAR3
IGROV1
HEY
F
PEO1
ES2
miNC
miR-517a
miNC
miR-517a
USP1
ID1
ID2
p21
archain 1
β-actin
G
miR-517a
ARCN1
Cell
Viability
USP1
ID 1/2
p21
Cell Cycle
Progression

Figure 2.4. miR-517a revealed a novel dependence on ARCN1 in ovarian cancer cells.

(A) Overexpression of a miR-517a mimic reduced cell viability in ovarian cancer cells (shown as EOC) but did not reduce viability in IHH and HOSE (shown as N). Each point represents the mean of 3 experiments, and the line represents the mean of all points in a column.

(B) Overexpression of a miR-517a mimic also reduced cell viability in a panel of 46 non-small cell lung cancer cell lines (shown as NSCLC) but did not reduce viability in normal bronchial epithelium (shown as HBEC). Each point represents the mean of 3 experiments, and the line represents the mean of all points in a column ± SD.

(C) In vivo delivery of neutral liposome incorporated miR-517a mimic reduced tumor burden in an orthotopic xenograft model using SKOV3 cells. Box-and-whisker plot of the range of values n=8 mice. p-value derived using Student's T-Test.

(D) The viability of depletion of predicted targets ARCN1 and USP1 in 12 NSCLC cell lines significantly correlated with viability upon overexpression of a miR-517a mimic. Each data point represents the mean of 3 experiments. R^2 generated using Pearson correlation.

(E) siRNA-mediated knockdown of ARCN1 closely phenocopied miR-517a mimic overexpression, and knockdown of USP1 decreased viability in one cell line (PEO1). Each data point represents a single experiment.

(F) Western blots showed expression of a miR-517a mimic reduced levels of predicted targets USP1 and ARCN1 in two cell lines. Decreased expression of ID1 and ID2 and induction of p21 expression was also observed upon miR-517a mimic expression.

(G) miR-517a reduced ovarian cancer cell viability by inhibiting expression of ARCN1 and USP1, which supports expression of ID proteins that inhibit p21 expression.

2.2.4 miR-124a Drives Cellular Differentiation in EOC Lines

miR-124a reduced viability in multiple ovarian cancer cell lines screened, but it did not reduce the viability of two normal cells lines, IHH and HOSE (Figure 2.5A). miR-124a displayed high penetrance in three non-clonal short-term culture cell lines, HCC5012, HCC5019, and HCC5030, and is reported to have decreased expression in serous ovarian tumors (Iorio et al., 2007). In order to determine downstream consequences of miR-124a expression, we performed a microarray experiment in PEO1 and PEO4 cells to identify genes with altered expression 72 hours after transfection with miR-124a mimic (Figure 2.5B). This experiment identified 2,904 genes with a 2-fold change in expression in PEO1 or PEO4 cells. Two previously published targets of miR-124a, CDK6 and NFKBIZ, were both downregulated greater than 2-fold on this microarray suggesting its ability to capture expression changes of miR-124a target mRNAs (Lindenblatt et al., 2009; Pierson et al., 2008). We then took advantage of the set of 124a-responsive genes in PEO1 cells to assess the predictive value of TargetScan (Lewis et al., 2003). Of the 1,131 genes that decreased expression 2-fold in PEO1 cells, we found that 460 were predicted targets in TargetScan, a significant enrichment with a p-value $< 10^{-6}$ (Figure 2.5C). Furthermore, we observed a strong correlation between total context score and the probability of decreased expression of a gene on the microarray, with predicted targets having context scores $\leq$ -0.2 showing a minimum 30% probability of displaying a 2-fold decrease in expression (Figure 2.5C). This analysis again confirmed the utility of seed-sequence based target prediction to determine functional outcomes of miRNA expression.

We then surveyed the microarray data to determine what the effects of miR-124a expression on ovarian cancer cells might be. miR-124a shares a seed sequence with miR-506, a miRNA previously reported to regulate an EMT network of genes in ovarian cancer (Yang et al., 2013). Furthermore, a previous study has shown that fibroblasts can be reprogrammed into neurons by overexpressing miR-124a (Xue et al., 2013). Consistent with these reports, we found that multiple mesenchymal markers decreased expression and multiple neuronal markers increased expression in both PEO1 and PEO4 cells upon miR-124a expression (Figure 2.5D). Mesenchymal markers included two predicted targets (Integrin β1 and Vimentin) and Twist2. Neuronal markers N-cadherin (CDH2), synaptobrevin (VAMP2), and MAP2 were upregulated as well (Figure 2.5D). Additionally, immunofluorescence demonstrated greatly increased expression of Tuj1 (TUBB3) and MAP2 (the two neuronal markers previously reported to be upregulated) in ES2 cells 48 hours after transfection with miR-124a mimic (Figure 2.5E). PTB and SCP1 are the reported miR-124a targets responsible for neuronal reprogramming of fibroblasts, and we observed significant decreases in expression of both on our microarray suggesting an intact neuronal differentiation circuit in EOC cell lines could be driven by miR-124a expression (Figure 2.5F).

We then assessed other predicted targets showing decreased expression on the microarray for functional consequences downstream of miR-124a. SIX4 is a homeodomain transcription shown to inhibit muscle satellite cell differentiation (Yajima et al., 2010). SIX transcription factors are known to bind to eyes absent homolog (EYA) proteins, which function

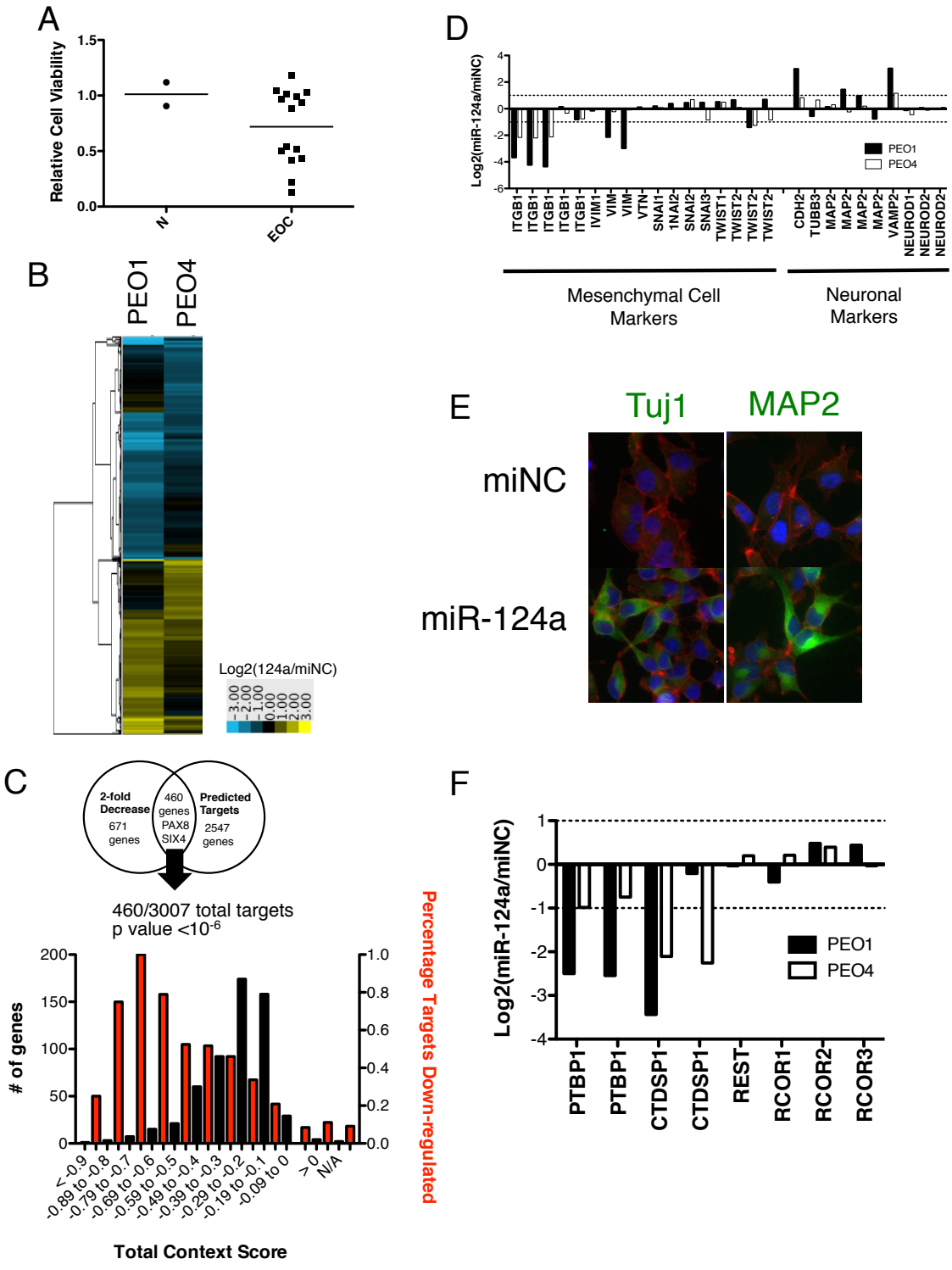
A
Relative Cell Viability
1.5
1.0
0.5
0.0
N
EOC
B
PEO1
PEO4
Log2(124a/miNC)
3.00
2.00
1.00
0.00
-1.00
-2.00
-3.00
C
2-fold Decrease 671 genes
460 genes PAX8 SIX4
Predicted Targets 2547 genes
460/3007 total targets
p value <10-6
# of genes
Percentage Targets Down-regulated
Total Context Score
D
Log2(miR-124a/miNC)
PEO1
PEO4
ITGB1 ITGB1 ITGB1 ITGB1 ITGB1 IVIM1 VIM VIM VTN SNAI1 1NAI2 SNAI2 SNAI3 TWIST1 TWIST2 TWIST2 TWIST2 CDH2 TUBB3 MAP2 MAP2 MAP2 MAP2 VAMP2 NEUROD1 NEUROD2 NEUROD2
Mesenchymal Cell Markers
Neuronal Markers
E
Tuj1
MAP2
miNC
miR-124a
F
Log2(miR-124a/miNC)
PEO1
PEO4
PTBP1 PTBP1 CTDSP1 CTDSP1 REST RCOR1 RCOR2 RCOR3

Figure 2.5. miR-124a reprogrammed ovarian cancer cells leading to aberrant induction of neuronal markers.

(A) Expression of miR-124a mimic reduced cell viability in ovarian cancer lines (EOC) but not in IHH or HOSE cells (shown as N). Each data point represents the mean of three experiments and the line represents the mean of all points in a column.

(B) miR-124a-responsive genes were identified by a unidirectional cluster of a whole genome expression microarray. This cluster was created using Euclidian distance of $\log_2$ of the ratio of gene expression upon miR-124a mimic expression to gene expression upon mimic negative control expression. Only genes with a 2-fold expression change in PEO1 or PEO4 were included.

(C) miR-124a responsive genes in PEO1 cells were enriched for TargetScan predicted targets. The probability that an expressed predicted target (defined as RPKM >0.8 in PEO1 cells) showed a 2-fold expression reduction decreased with increasing total context score. p-value derived from hypergeometric distribution.

(D) miR-124a mimic expression reduced expression of mesenchymal markers ITGB1, VIM, and TWIST2 and increased expression of neuronal markers CDH2, VAMP2, and MAP2 according to microarray data. Each bar represents the log2 of the ratio of the means of three experiments of mir-124a mimic expression to mimic negative control expression of a single probe on the microarray.

(E) Immunofluourescence images of ES2 cells transfected with miR-124a mimic showed increased expression of neuronal marker proteins Tuj1 (TUBB3) and MAP2 48 hours after transfection. Cells were counterstained with DAPI and Texas Red-conjugated phalloidin. **(F)** Expression of miR-124a mimic reduced expression of PTBP1 (PTB) and CTDSP1 (SCP1) but not other members of the REST complex on a microarray. Each bar represents the $\log_2$ of the ratio of the means of three experiments of mir-124a mimic expression to mimic negative control expression of a single probe on the microarray.

as coactivators of these transcription factors (Ohto et al., 1999). SIX4 and all four isoforms of EYA proteins are predicted to be targets of miR-124a (Figure 2.6A); therefore, it seemed possible that miR-124a might also target this transcriptional circuit. Microarray data indicated that only SIX4 was downregulated in response to miR-124a expression, so we focused on this transcription factor.

Mining of TCGA expression data from serous ovarian adenocarcinomas revealed that SIX4 showed significantly increased expression in ovarian tumors relative to unmatched normal ovarian tissue (Figure 2.6B). Western blots showed that SIX4 protein levels decreased upon miR-124a expression in multiple ovarian cancer cell lines, so we investigated if SIX4 supported ovarian cancer cell survival (Figure 2.6C). siRNA-mediated knockdown of SIX4 showed that depletion of this transcription factor could phenocopy miR-124a overexpression in PEO1 cells (Figure 2.6D). Investigation of the penetrance of SIX4 depletion found that SIX4 knockdown greatly reduced cell viability in multiple EOC cell lines while remaining relatively innocuous in HOSE cells (Figure 2.6E). In order to assess if depletion of SIX4 could affect tumor growth in vivo, we performed an experiment similar to the in vivo delivery of miR-517a, but here we seeded tumors by intraperitoneal injection of ES2 cells. Tumors were allowed to form over the course of seven days before delivery of DOPC neutral liposomal incorporated SIX4 siRNA or negative control siRNA. After 4 weeks of treatment, examination showed a decrease in tumor burden in SIX4-treated mice, seen through decreased tumor weight and ascites volume (Figure

2.6F). Thus, SIX4 was found to be overexpressed in ovarian tumors and supported ovarian tumor growth in an orthotopic xenograft model.

To further investigate the effects of SIX4 depletion in ovarian cancer cells, we queried the manner of cell viability reduction upon SIX4 knockdown. Using the luminescent reagent CaspaseGlo 3/7, we found that cells treated with SIX4 siRNA did not show increased caspase activity 48 hours after knockdown (Figure 2.6G). However, a BrdU incorporation assay revealed appreciably less BrdU incorporation in ES2 cells 48 hours post-transfection (Figure 2.6G). We also conducted propidium iodide staining and performed DNA content and cell cycle analysis at the same time point. This assay showed significantly fewer cells in S-phase than cells treated with a negative control siRNA suggesting a G1 cell cycle block (Figure 2.6G). The sum of these data suggested that SIX4 depletion decreased cell viability via a cytostatic mechanism.

In order to identify downstream effectors of SIX4, we performed a whole genome expression array in PEO1 and PEO4 cells transfected with negative control siRNA and SIX4 targeted siRNA (Figure 2.7A). This microarray revealed 3059 genes with 2-fold alteration in expression upon SIX4 depletion in PEO1 or PEO4 cells. Microarray data demonstrated that expression of multiple cyclins, including cyclin E1, cyclin E2, and cyclin D2, decreased upon knockdown of SIX4 (Figure 2.7B). This decrease in cyclin expression could, in part, explain the decrease in cells in S-phase. We also observed that decreased SIX4 expression induced expression of STRADB in both PEO1 and PEO4 (Figure 2.7C). STRADB functions to stabilize LKB1 expression and activate signaling along the AMPK signaling pathway. However, neither

A

Gene	Conserved 8mer Sites	Conserved 7mer Sites	Context Score
SIX4	1	2	-0.72
EYA4	2	0	-0.60
EYA2	1	0	-0.31
EYA1	1	0	-0.18
EYA3	1	0	-0.14

B

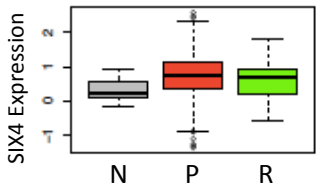

Tumor vs. normal p-value = 0.0161

C

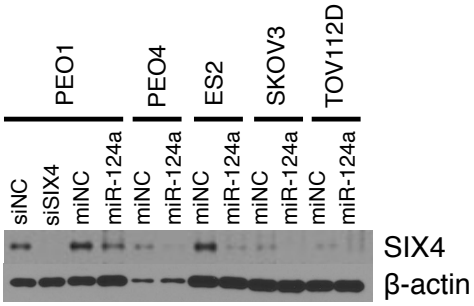

D

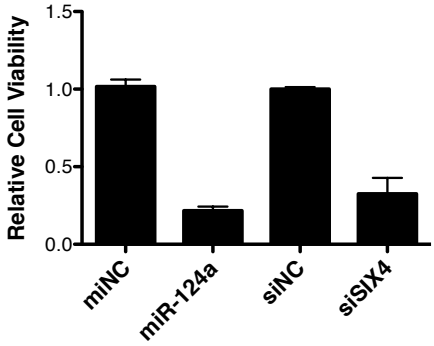

E

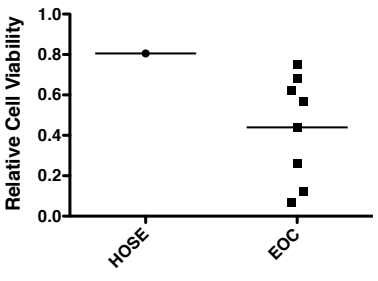

F

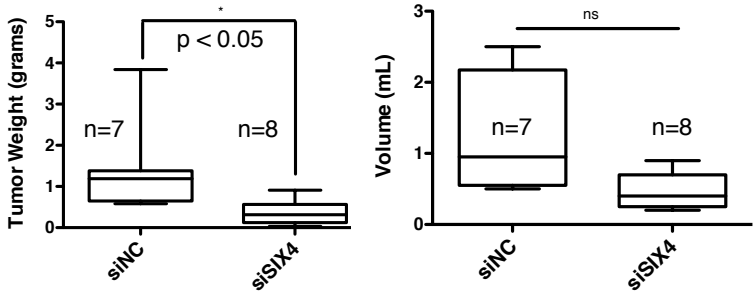

G

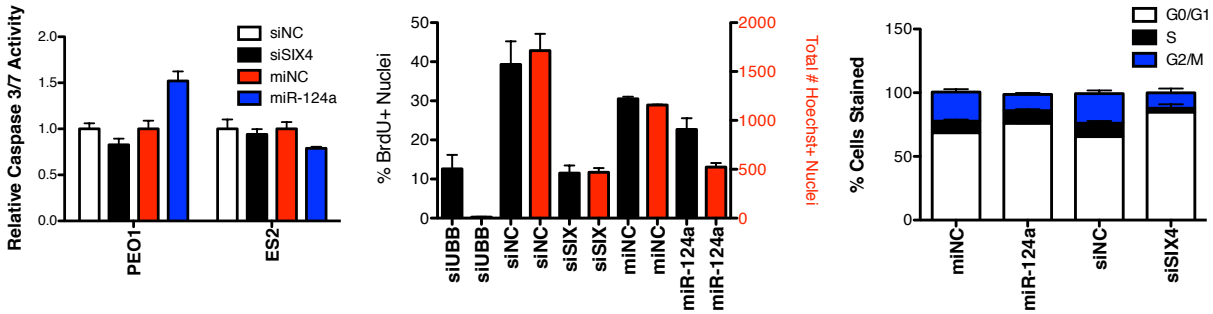

Figure 2.6. miR-124a reduced expression of SIX4, a transcription factor with increased expression in ovarian tumors.

(A) SIX4, EYA1, EYA2, EYA3, and EYA4 are predicted targets of miR-124a in TargetScan (www.targetscan.org).

(B) SIX4 expression was significantly increased in human ovarian tumors relative to unmatched normal ovarian tissue. p-value from Welch two sample T-test.

(C) Western blots showed expression of a miR-124a mimic reduced levels of SIX4 protein in five ovarian cancer cell lines.

(D) Knockdown of SIX4 reduced cell viability similar to expression of a miR-124a mimic in PEO1 cells (mean ± SD of 3 experiments).

(E) Depletion of SIX4 expression reduced cell viability in multiple ovarian cancer lines (shown as EOC) but minimally reduced viability in HOSE cells. Each point represents the mean of 3 experiments with the lines representing the mean of all points in a column.

(F) *in vivo* knockdown of SIX4 using neutral liposome incorporated siRNA reduced tumor burden and ascites volume in an orthotopic xenograft mouse model using ES2 cells. Box-and-whisker plot of the range of values of n=8 mice. p-value derived using Student's T-Test.

(G) SIX4 knockdown did not induce activation of caspase 3 and caspase 7. Depletion of SIX4 reduced BrdU incorporation in ES2 cells resulting in decreased Hoechst-positive nuclei 48 hours post-transfection. SIX4 knockdown also resulted in decreased cells in S-phase as seen in PI stained ES2 cells 48 hours post-transfection. All bars represent the mean ± SD of 3 experiments.

STRADA nor any other member of the AMPK signaling was significantly upregulated in addition to STRADB. One role of STRAD-induced AMPK signaling is cellular polarization and the formation of epithelial cell junctions (Zhang et al., 2006). E-cadherin staining in PEO1 cells 48 hours after SIX4 knockdown revealed increased membrane-associated E-cadherin and formation of cell adhesions, suggesting depletion of SIX4 was sufficient to re-establish an epithelial phenotype in these cells (Figure 2.7D). Furthermore, western blots showed stabilization of LKB1 and MO25, increased activating phosphorylation of AMPK at T172, and increased phosphorylation of acetyl-CoA carboxylase (ACC) downstream of AMPK (Figure 2.7E). These data suggested that SIX4 both promoted cell cycle progression, possibly by increasing expression of cyclins, and also inhibited signaling down the tumor suppressive AMPK pathway. miR-124a then inhibited two separate inhibitors of cell differentiation: SCP1, which inhibits neuronal differentiation as part of the REST complex, and SIX4, which inhibited epithelial differentiation by inhibiting the AMPK signaling pathway (Figure 2.7F).

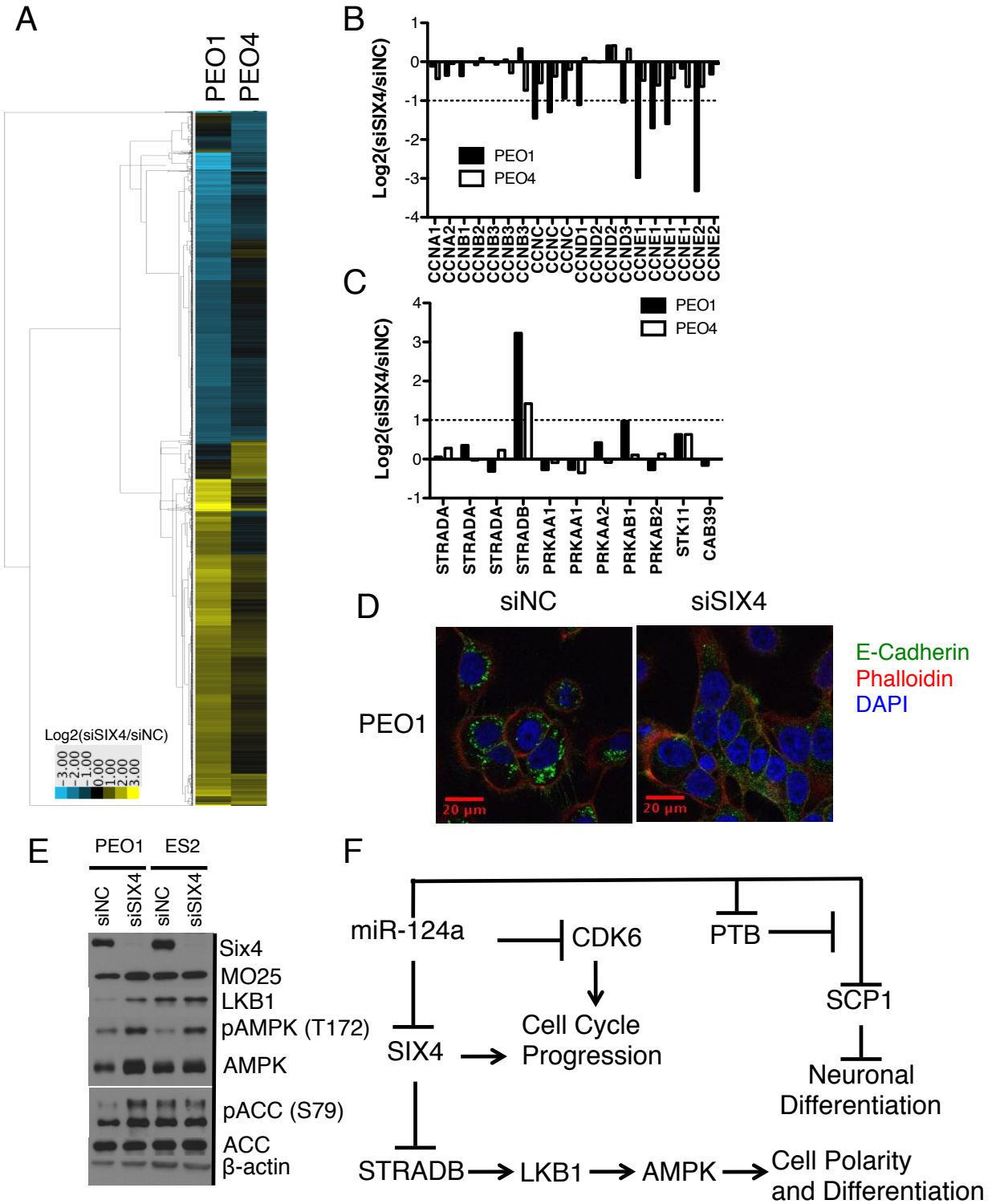
A
PEO1
PEO4
Log2(siSIX4/siNC)
−3.00
−2.00
−1.00
0.00
1.00
2.00
3.00
B
Log2(siSIX4/siNC)
PEO1
PEO4
CCNA1
CCNA2
CCNB1
CCNB2
CCNB3
CCNB3
CCNC
CCNC
CCND1
CCND2
CCND2
CCND3
CCNE1
CCNE1
CCNE1
CCNE2
CCNE2
C
Log2(siSIX4/siNC)
PEO1
PEO4
STRADA
STRADA
STRADA
STRADB
PRKAA1
PRKAA1
PRKAA2
PRKAB1
PRKAB2
STK11
CAB39
D
siNC
siSIX4
PEO1
20 μm
20 μm
E-Cadherin
Phalloidin
DAPI
E
PEO1
ES2
siNC
siSIX4
siNC
siSIX4
Six4
MO25
LKB1
pAMPK (T172)
AMPK
pACC (S79)
ACC
β-actin
F
miR-124a
CDK6
PTB
SCP1
SIX4
Cell Cycle
Progression
Neuronal
Differentiation
STRADB
LKB1
AMPK
Cell Polarity
and Differentiation

Figure 2.7. SIX4 depletion activated the AMPK pathway resulting in epithelial differentiation of ovarian cancer cells.

(A) SIX4-responsive genes were identified by a unidirectional cluster of a whole genome expression microarray. This cluster was created using Euclidian distance of $\log_2$ of the ratio of gene expression with siSIX4 transfection to negative control transfection. Only genes with a 2-fold expression change in PEO1 or PEO4 were included.

(B) Knockdown of SIX4 reduced expression of multiple cyclin proteins in PEO1 and PEO4 cells on the microarray. Each bar represents the $\log_2$ of the ratio of the means of three experiments of SIX4 siRNA transfection to siRNA negative control transfection of a single probe on the microarray.

(C) SIX4 knockdown induced expression of STRADB in PEO1 and PEO4 cells according to microarray data. Each bar represents the $\log_2$ of the ratio of the means of three experiments of SIX4 siRNA transfection to siRNA negative control transfection of a single probe on the microarray.

(D) SIX4 knockdown resulted in relocalization of E-cadherin to the cell membrane and formation of cell adhesions in ES2 cells 48 hours after transfection. Cells were stained for E-cadherin and counterstained with Texas Red-conjugated phalloidin and DAPI.

(E) Western blots showed SIX4 knockdown resulted in increased LKB1 and MO25 protein and increased activating phosphorylation of AMPK. Increased AMPK activity was seen through increased phosphorylation of acetyl-CoA carboxylase (ACC).

(F) miR-124a drove a cell differentiation program by inhibiting multiple inhibitors of cell differentiation including SIX4, which promoted cell cycle progression and inhibited signaling through the tumor suppressive AMPK pathway, and SCP1, an inhibitor of neuronal differentiation.

2.3 Discussion

2.3.1 Ovarian Cancer Has a Diverse Landscape of Vulnerabilities

The screen performed here revealed the highly idiosyncratic nature of vulnerabilities in ovarian cancer cell lines. Each cell line possessed a unique toxicity profile, though some hits were common across multiple cell lines. The topography of vulnerabilities validated our use of multiple cell lines, as many toxic miRNAs would not have been identified if only a single cell line had been used. Furthermore, this screen suggested that a panel of cell lines might be able to accurately recapitulate some of the biology of ovarian cancer. Because the idiosyncratic nature of most hits observed might be due to cell culture artifacts, we investigated if these hits might play some role in the disease. Two idiosyncratic hits identified by the screen appeared to be relevant to the disease as higher expression of both miR-505 and miR-146a was found to correlate with increased patient survival. These miRNAs have previously been shown to correlate with a better prognosis as part of a multi-miRNA signature, but neither was shown to have power as a single agent as was shown here (Creighton et al., 2012). Correlation between miR-146a and patient prognosis and observation of reduced viability of ovarian cancer cells upon miR-146a transfection is consistent with previous reports which observe this miRNA exerting tumor suppressive effects in other cancer types. Loss of miR-146a has been shown to lead to formation of hematological malignancies in mice, and this miRNA has been suggested to play a tumor suppressive role in multiple cancer backgrounds (Chen et al., 2013; Li et al., 2012; Zhao et al., 2011). Additionally, a polymorphism has been identified in the gene encoding this

miRNA, though a study suggests that this polymorphism does not play a role in ovarian cancer formation (Garcia et al., 2011b; Jazdzewski et al., 2008; Shen et al., 2008; Yamashita et al., 2013). Again arguing for the relevance of idiosyncratic hits, multiple miRNAs with decreased expression in serous ovarian tumors were hits in new non-clonal cell lines generated to more closely mirror tumors. Specific hits might reflect some of the biological heterogeneity of this disease, and therefore might not be expected to display great penetrance throughout the panel of cell lines. The landscape of vulnerabilities observed in this screen suggests that the "turbulent genome" thought to be driving ovarian tumor progression leads to multiple, unique vulnerabilities. However, the identification of hits with greater penetrance suggests that some vulnerabilities can be distilled down to a few, common linchpin processes.

2.3.2 Unique Biology Drives Specificity of miRNA Toxicity

Investigation into the factors driving mimic specificity revealed that idiosyncratic hits were not driven by dosage effects or expression of their respective endogenous miRNAs. Unique biology appeared to be the basis of idiosyncratic hits, again addressing the enormous amount of diversity found in ovarian tumors. Also, the manifold biology of ovarian tumors implies the necessity of personalized therapy in this disease setting. We then focused on utilizing high-resolution genomic data from two related cell lines, PEO1 and PEO4, to parse out if a line's genetic background defined sensitivity to a mimic. Though we were unable to completely define the specificity of two PEO4-specific hits, miR-155 and miR-181b, we did

uncover functional consequences of expression of these miRNAs using tools which looked for enrichment of computationally predicted targets in annotated gene sets (Lu et al., 2012; Papadopoulos et al., 2009). Both miRNAs inhibited signaling by the AKT pathway and appeared to lead to internalization of membrane-associated E-cadherin. Though neither of these two effects conclusively explained specificity of toxicity, they did show an ability to deconvolute target space of a miRNA into discrete functional consequences of miRNA expression.

High-resolution genomic sequencing also provided insight into the amount of dissimilarity between the PEO1 and PEO4 cell lines. The large number of SNVs unique to each line spoke to great diversity of biology present within a single ovarian tumor. The combination of differences in SNVs, CNVs, and transcriptomes suggested fundamental biological differences between these two cell lines. At least one of these distinctions was found to be a discrepancy in epithelial and mesenchymal status. Surprisingly, the more epithelial-appearing line, PEO4, was also the more drug resistant line. Treatment of ovarian tumors with platinum and taxanes applies tremendous selective pressure, and perhaps also provides selective advantages to cells that would otherwise be out-competed. Extinction of competitive clones from a tumor due to treatment might open space, which a less competitive, but more drug-resistant, clone could fill. If so, a greater understanding of the evolution of a single tumor will allow for more rational approaches to treatment to prevent disease recurrence and the appearance of resistance to drugs.

2.3.3 Penetrant Hits Uncover New Biology Supporting Ovarian Cancer Cell Survival

miR-517a reduced cancer cell viability in vitro and reduced tumor burden in vivo. The ability of miR-517a to reduce viability in both EOC and NSCLC cell lines suggested its ability to regulate processes critical to cancer cell survival in a broader sense. This finding is consistent with reports that miR-517a expression can act in a tumor suppressive manner in bladder and hepatocellular cancers (Liu et al., 2013; Yoshitomi et al., 2011). However, miR-517a was not toxic in normal immortalized cell lines, either ovarian or bronchial, so it does not target a process required in all cells. Depletion of ARCN1, which encodes a member of the coatamer complex, was observed to be responsible for the miR-517a phenotype in ovarian cancer cells, while depletion of both ARCN1 and USP1 could copy the phenotype of miR-517a in NSCLC lines. This data suggested that miR-517a targeted both a broadly important process and a background-specific process. miR-21 has been shown to target multiple inhibitors of AKT signaling to better act as a rheostat of this pathway (Hatley et al., 2010). Interestingly, miR-517a is not predicted to target any other members of the coatamer complex besides ARCN1. Either ARCN1 is an exquisitely sensitive node ideal for regulation of this complex, or there are novel, as yet undiscovered, functions of this gene. Either way, more investigation is necessary to determine the manner in which ARCN1 depletion reduces cancer cell viability as this mechanism appears to broadly support cancer cell survival. USP1 has been shown to support an undifferentiated, stem-cell like phenotype in osteosarcoma cells (Williams et al., 2011). While only one ovarian cancer cell line was sensitive to depletion of USP1, multiple NSCLC lines showed reduced

viability suggesting this deubiquitinase's importance in other settings. A greater understanding of the factors defining sensitivity to USP1 depletion could be important, as deubiquitinases have been shown to be druggable targets (Chauhan et al., 2012; Reverdy et al., 2012).

2.3.4 A miRNA and Its Client Transcription Factor Drive Differentiation of Ovarian Cancer Cells

miR-124a reduced cell viability in multiple EOC cell lines, and perhaps more importantly showed penetrance in all 3 newly-derived non-clonal, short-term culture cell lines. Consistent with the observed reduction in cancer cell viability, hypermethylation of this miRNA in acute lymphocytic leukemia and decreased expression in hepatocellular carcinoma correlates with a poor prognosis (Agirre et al., 2009; Zheng et al., 2012). miR-124a has also been found to have decreased expression in serous ovarian adenocarcinoma (Iorio et al., 2007). A miRNA sharing the same seed sequence as miR-124a, miR-506, regulates a gene network that leads to epithelial-mesenchymal transition (EMT) in ovarian cancer cells (Yang et al., 2013). Consistent with this observation, a microarray revealed that expression of this miRNA led to decreased expression of mesenchymal markers. Two mesenchymal markers downregulated by miR-124a, vimentin and integrin β1, are predicted targets suggesting direct regulation of these genes by miR-124a. Furthermore, decreased expression of the transcription factor Twist2 also suggested that miR-124a could regulate EMT in ovarian cancer cells. We also observed that miR-124a expression led to increased neuronal markers N-cadherin, synaptobrevin, TUBB3, and MAP2 in ovarian

cancer cells. Consistent with the induction of neuronal markers observed, miR-124a has been shown to reprogram fibroblasts to adopt a neuronal fate (Xue et al., 2013). Decreased expression of PTB and SCP1 suggested that the transcriptional circuit responsible for fibroblast reprogramming was also targeted in ovarian cancer cells. It seemed somewhat surprising that a single perturbation was able to reprogram ovarian cancer cells, reducing mesenchymal markers and leading to neuron-like phenotype.

We then utilized a microarray to identify other miR-124a-responsive genes that might be downstream effectors of mimic expression. SIX4 deletion in mice has been suggested to play a role in muscle cell development, with one report suggesting that SIX4 inhibits satellite cell differentiation (Liu et al., 2010; Niro et al., 2010; Yajima et al., 2010). Therefore, we were interested whether miR-124a might inhibit SIX4 to drive cellular differentiation. This transcription factor was found to have reduced expression upon miR-124a expression by western blotting, and depletion of SIX4 displayed a penetrant phenotype in multiple EOC cell lines, reducing cell viability via a cytostatic mechanism. Consistent with this mechanism, we found reduced expression of cyclin genes after knockdown of SIX4 expression. We also observed induction of STRADB and increased activity of the AMPK pathway after SIX4 knockdown, suggesting SIX4 also negatively regulates signaling of this pathway. Consistent with increased AMPK signaling, reduction of SIX4 expression led to increased cell adhesion and relocalization of E-cadherin to the cell membrane. Thus, SIX4 overexpression in tumors might function as "two hits" in a tumor cells, driving cell proliferation and reducing signaling along the tumor

suppressive AMPK pathway. Suggesting that SIX4 might play a role in ovarian tumor progression, we observed increased expression of SIX4 in ovarian tumors relative to normal tissue and depletion of SIX4 reduced tumor burden in vivo. SIX4 might be needed to drive proliferation, evade AMPK signaling, or to maintain an undifferentiated state in ovarian cancer cells. Further investigation is necessary to determine the effects of SIX4 overexpression in these cells. Thus, miR-124a might also drive a differentiation program by reducing levels of SIX4, which blocked epithelial differentiation via the AMPK pathway in ovarian cancer cells.

Both miR-517a and miR-124a appeared to drive cell differentiation programs. Overexpression of both of these miRNAs reduced cell viability, suggesting the possibility that differentiation therapy might be a viable treatment option for ovarian cancer. Perhaps the most widely successful and well-known example of differentiation therapy is the treatment of acute promyelocytic leukemias (APMLs) with all trans-retinoic acid (ATRA). This treatment functions in a cancer where almost all patients share a chromosomal rearrangement (de The et al., 1990; Larson et al., 1984). While differentiation therapy has often been discussed as a strategy for treatment of cancers, the only proven efficacious treatments have occurred in relatively simple genetic backgrounds. However, the work presented here suggests that differentiation therapy might be a viable treatment strategy even in the background of numerous, complex, and diverse genetic abnormalities. Given the evolution of the tumor giving rise to PEO1 and PEO4 cells, differentiation therapy might prove more efficacious than current cytotoxic therapies. If terminal differentiation of all remaining cancer cells could be achieved

after surgical debulking, disease progression would halt and no extinction event would occur providing a niche for continued growth and evolution of the tumor.

2.4 Methods and Materials

Cell Culture

PEO1 and PEO4 cells were generously provided by Hani Gabra (University of Edinburgh Cancer Research Center). ES2 and TOV112D cell lines were purchased from the ATCC. SKOV3, Hey, OC316, OVCAR3, A2780, EFO21, EFO27, OAW42, and UPN251 cell lines were generously provided by Dr. Robert Bast (MD Anderson Cancer Center). IHH cells were generously provided by Dr. John Abrams (UT Southwestern). HOSE cells were generously provided Dr. William Hahn (Dana Farber Cancer Institute, Harvard). PEO1, PEO4, SKOV3, ES2, TOV112D, Hey, OC316, OVCAR3, A2780, EFO21, EFO27, OAW42, and UPN251 cell lines were grown in RPMI medium with l-glutamine and 25mM HEPES (Gibco) supplemented with 10% fetal bovine serum (Atlanta Biologicals) and 100 U/mL penicillin and 100 µg/mL streptomycin (Gibco). HCC5012, HCC5030, and HCC5019 were grown in ACL4 medium supplemented with 5% fetal bovine serum (Atlanta Biologicals). HOSE cells were grown in Keratinocyte Serum Free Medium with supplements (Gibco) and 100 U/mL penicillin and 100 µg/mL streptomycin (Gibco). IHH cells were grown in DMEM medium (Gibco) supplemented with 10% fetal bovine serum (Atlanta Biologicals) and 100 U/mL penicillin and 100 µg/mL streptomycin (Gibco). Transfections were performed as described in the miRNA mimic screens.

miRNA Mimic Screens and Transfection

All cell lines were screened using a collection of miRNAs consisting of the intersection of two Dharmacon miRIDIAN Mimic Libraries inclusive of all miRNAs annotated in miRBase 8.0 and miRBase 10.1 respectively (www.mirbase.org). Screens were performed similarly to those previously described with slight modifications (Ganesan et al., 2008; Whitehurst et al., 2007). 10 picomoles of miRNA mimic were plated in 30 μL serum free medium using a Biomek FX robotic liquid handler (Beckman Coulter). 9.8 μL of serum free medium containing 0.2 μL of RNAiMax transfection reagent was then added to each well using a TiterTek multidrop (except for PEO4 where 0.2 μL of DharmaFECT 3 was used). The plates were then allowed to incubate for 20-30 minutes at room temperature before cells were plated. Using a trypsin-mediated single-cell suspension, cells were plated in each well using a TiterTek multidrop to a total volume of 150 μL. Cell lines were plated with the total number of cells per well as follows: PEO1 (10,000), PEO4 (10,000), SKOV3 (5000), A2780 (20,000), OC316 (5000), EFO21 (5000), Hey (5000), OVCAR3 (12,500), IGROV1 (12,500), EFO27 (15,000), UPN251 (10,000), OAW42 (10,000), and CAOV3 (5000). All cells were plated in the media in which they were grown as described above. Plates were then centrifuged at 500 RPM for 1 minute and incubated in a 37°C/5% CO2 incubator. 72 hours after plating cells 50 μL of fresh media was added to each well using a TiterTek multidrop. 120 hours after plating, 15 μL of CellTiter-Glo Reagent (Promega) was added to each well and incubated per manufacturer's protocol. Luminescence

values for each well were then recorded using an Envision Plate Reader (Perkin Elmer). Each transfection was performed in triplicate. Transfection of siRNAs was performed as described above using 10 pmoles of a pooled siRNA instead of miRNA mimic. HOSE and IHH transfection were performed as above plating 10,000 cells per well and 2,000 cells per well respectively.

Data Normalization

Raw luminescence values for each well were normalized to allow for comparisons from well to well and plate to plate. Each well in a row was normalized to the median value for the row. The Z-score for each well was then derived using the siMACRO macro for excel (Singh et al., 2013). Mimics which resulted in Z-scores ≤ -2 were considered as hits for each screen.

Antibodies

Antibodies were purchased from Cell Signaling (pAKT (T308) #2965, pAKT (S473) #4060, panAKT #4691, pGSK3β (S9) #9327, GSK3β #9315, p27 #3686, TSC2 #3635, pMEK (S217/221) #9121, MEK1/2 #9122, ERK1/2 #9102, pERK (T202/Y204) #4370, SMAD4 #9515, pSMAD3 (S423/425) #9520, SMAD3 #9523, SMAD2 #5339, USP1 #8033, p21 #2947, LKB1 #3050, pAMPK (T172) #2535, AMPK #2532, pACC (S79) #3661, ACC #3676), Sigma (β-actin #A1978), Millipore (pSMAD2 (S465/467) #AB3849), Santa Cruz (ID1 #SC-488 and ID2 #SC-489), Novus (SIX4 #51804-M09 and ARCN1 #NBP1-32377), and Epitomics (MO25 #2027-1).

HRP-conjugated secondary antibodies were purchased from Jackson Immunolaboratories, and ECL reagents were purchased from ThermoScientific.

Immunofluorescence

Cells were subjected to reverse transfection as described and plated on coverslips. After 48 hours, cells were washed with PBS and fixed with 4% methanol-free formaldehyde (Fisher). Cells were then permeabilized with 0.5% Triton-X 100 in PBS. Manufacturer's protocols were then followed for blocking and incubation with primary antibodies except all primary antibodies were used at 1:100 dilution. Primary antibodies were purchased from BD Biosciences (E-cadherin #610181) and Covance (Tuj1 #MMS-435P and MAP2 #SMI-52R). Cells were then incubated with Alexa 488-conjugated secondary antibodies (Invitrogen) at 1:500 for 1 hour at room temperature. Coverslips were then stained with Texas Red-X phalloidin per manufacturer's protocol (Invitrogen #T7471). Coverslips were then mounted onto slides using Vectashield (Vector Labs) mounting medium containing DAPI. Slides were imaged using a TCS SP5 confocal microscope using a sequential 3-channel scan. Tuj1 and MAP2 staining was imaged using a Zeiss Axioplan 2E with a Hammamatsu monochrome digital camera. OpenLab (Improvision) software was used for image acquisition on the Zeiss microscope. All image processing was conducted in ImageJ.

Animals, orthotopic in vivo model and tissue processing.

Female athymic nude mice were purchased from the National Cancer Institute, Frederick Cancer Research and Development Center (Frederick, MD). These animals were cared for according to guidelines set forth by the American Association for Accreditation of Laboratory Animal Care and the U.S. Public Health Service policy on Human Care and Use of Laboratory Animals. All mouse studies were approved and supervised by the M.D. Anderson Cancer Center Institutional Animal Care and Use Committee. All animals used were between 8-12 weeks of age at the time of injection. For the miR-517a experiment, SKOV3ip1 cells were trypsinized, washed and resuspended in Hanks' balanced salt solution (Gibco, Carlsbad, CA) and injected intraperitoneally into mice (SKOV3ip1: $1x10^6$ cells/animal). Similarly, for the SIX4 siRNA experiment, ES2 cells ($2.5x10^5$ cells/animal) were prepared and injected intraperitoneally. For both experiments, seven days after the tumor cell injection, mice were randomly divided and treated with oligonucleotides incorporated in neutral nanoliposomes (intraperitoneal [IP] administration). For the miR-517a experiment, mice were randomized to the following three groups (n = 10/group): negative control miRNA/DOPC or miR-517a/DOPC at either 200 μg/kg or 400 μg/kg. For the SIX4 experiment, mice were randomized to the following two groups (n = 10/group): negative control siRNA or SIX4 siRNA. For both experiments, twice weekly treatments continued for 4-5 weeks at which point, all mice in the experiment were sacrificed and necropsied, and tumors were harvested. Tumor weights, number and location of tumor nodules were recorded. Tumor tissue was either fixed in formalin for paraffin embedding, frozen in optimal cutting temperature (OCT) media to prepare frozen slides, or snap frozen for lysate

preparation.

Liposomal preparation. miRNA for *in vivo* delivery was incorporated into DOPC as previously described (Landen et al., 2005). DOPC and miRNA were mixed in the presence of excess tertiary butanol at a ratio of 1:10 (w/w) miRNA/DOPC. Tween 20 was added to the mixture in a ratio of 1:19 Tween 20:miRNA/DOPC. The mixture was vortexed, frozen in an acetone/dry ice bath and lyophilized. Before in vivo administration, this preparation was hydrated with PBS at room temperature at a concentration of 200 µg/kg per injection.

miRNA mimics and siRNA Oligos

miRNA miRIDIAN mimics were purchased from Dharmacon (Mimic Negative Control #1, hsa-miR-210, hsa-miR-155, hsa-miR-181b, hsa-miR-517a, hsa-miR-124a). siGENOME siRNA oligos were purchased from Dharmacon (Non-targeting Pool #2, PTEN, AKT3, SMAD2, SMAD3, USP1, SIX4). MISSION oligos from Sigma (AKT1 [SASI_Hs01_00205545 , SASI_Hs01_00205546, SASI_Hs01_00205547], AKT2 [SASI_Hs01_00035058, SASI_Hs01_00035055, SASI_Hs01_00035057], and ARCN1 [SASI_Hs02_00332254, SASI_Hs01_00205402, SASI_Hs01_00205403]) For animal experiments miRNA mimics were purchased from Dharmacon and siRNA oligos from Sigma (SIX4 #SASI_Mm01_00078274 and MISSION siRNA Universal Negative Control #1).

Sequences:

hsa-miR-210 –

5’-CUGUGCGUGUGACAGCGGCUGA-3’

hsa-miR-155 –

3’-UUAAUGCUAAUCGUGAUAGGGGU-3’

hsa-miR-181b –

3’-AACAUUCAUUGCUGUCGGUGGGU-3’

hsa-miR-517a –

3’-AUCGUGCAUCCCUUUAGAGUGU-3’

hsa-miR-124a –

3’-UAAGGCACGCGGUGAAUGCC-3’

PTEN –

5’-GUGAAGAUCUUGACCAAUG-3’

5’-GAUCAGCAUACACAAAUUA-3’

5’-GGCGCUAUGUGUAUUAUUA-3’

5’-GUAUAGAGCGUGCAGAUAA-3’

AKT3 –

5’-GAAAGAUUGUGUACCGUGA-3’

5’-GGACUACUGUUAUAGAGAG-3’

5’-UGAGACAGAUACUAGAUAU-3’

5’-GCUCAUUCAUAGGAUAUAA-3’

SMURF2 –

5’-GAUGAGAACACUCCAAUUA-3’

5’-GACCAUACCUUCUGUGUUG-3’

5’-CAAAGUGGAAUCAGCAUUA-3’

5’-GAACAACACAAUUUACAGA-3’

SMAD2 –

5’-GAACAAACCAGGUCUCUUG-3’

5’-GCAGAACUAUCUCCUACUA-3’

5’-GAAGAGGAGUGCGCUUAUA-3’

5’-GGUGUUCGAUAGCAUAUUA-3’

SMAD3 –

5’-UCAAGAGCCUGGUCAAGAA-3’

5’-GAGUUCGCCUUCAAUAUGA-3’

5’-GGACGCAGGUUCUCCAAAC-3’

5’-GGACGAGGUCUGCGUGAAU-3’

USP1 –

5’-GCAUAGAGAUGGACAGUAU-3’

5’-GAAAUACACAGCCAAGUAA-3’

5’-CAUAGUGGCAUUACAAUUA-3’

5’-GCACAAAGCCAACUAACGA-3’

SIX4 –

5’-CCAGUGGAGUUAUCCUUAA-3’

5’-GAUGGAGGGUCUGUAGUGA-3’

5’-UGUCUUAGAUGGCAUGGUU-3’

5’-GUAUACACGGUUCCUAAUA-3’

Animal Experiments

SIX4 from Sigma –

SASI_Mm01_00078274 5’-CUUAAUGAUGCUGGACUCU-3’

High Resolution Genomic Sequencing

Exome Sequencing

For each cell line, 5 ug of genomic DNA was isolated and subjected to whole exome sequencing. In brief, DNA was fragmented (150-250 bp) and ligated to the paired-end adaptors. The adaptor-ligated fragments were then amplified by PCR and purified. Exon-containing fragments in these libraries were hybridized to the SureSelect Human All Exon Kit from Agilent technologies. This kit targets 165,637 exons (approx. 18,003 genes), totaling approximately 38 Mb of genomic DNA. The hybridized fragments were then captured using streptavidin coated magnetic beads, amplified and each sample was sequenced in the UT Southwestern Genomics Core Facility in two lanes of an Illumina GAIIx using a standard 75-bp paired-end protocol. The image analysis

and base calling were performed using the Illumina pipeline with default settings. Prior to analysis, duplicate reads (multiple fragments from the same amplicon), identified on the basis of having the same start position for both end reads, were removed from the sequence analysis. For copy number analysis, a total of 88 million read pairs (2 X 74 bp) for PEO1 and 89 million read pairs for PEO4 passed QC, and 148 million reads from each of the two lines were uniquely aligned to NCBI human genome build 37 by Bowtie 0.12.5 (Langmed B et al. Genome Biology) allowing up to 2 mismatches per read. Genome-wide copy number variation was analyzed for the pair of cell lines separately using completely unrelated normal tissue data obtained by others with the same exome-capture kit as a reference for normalization.

RNA Sequencing

RNA was isolated in triplicates from PE01 and PE04 cell lines using the RNAEasy Kit (Qiagen) and the quality of RNA was checked using a Bioanalyser. From each sample, 5 ug of RNA was used to perform RNA-Seq using the Illumina mRNA Sequencing Sample Preparation Guide (Illumina, Cat # RS-930-1001). First poly-A containing mRNA was purified using poly-T oligo attached magnetic beads and then fragmented using divalent cations under elevated temperatures. Then the first and second strand cDNA was synthesized using random primers, end-repaired, adenylated and ligated with paired-end adapters. The products were then purified and enriched with PCR to create the final cDNA library. The library from each sample was sequenced in a single lane of an Illumina GAIIx using a standard 40-bp paired-end protocol. Reads were

mapped to the UCSC *Homo sapiens* reference genome hg19 and their relative expression values were calculated in RPKM using CLC Biosystems Genomic Workbench software.

Whole Genome Expression Microarrays

RNA was isolated from cells 72 hours post-transfection using an RNAEasy kit (Qiagen). Illumina HumanWG-6 V4 BeadChip (Illumina, Inc.) human whole-genome expression arrays, which contain 47,231 probes on each array, were used. Each RNA sample was amplified by Ambion TotalPrep RNA amplification kit with biotin UTP (Enzo) labeling, using 500 ng of total RNA. The Ambion Illumina RNA amplification kit uses T7 oligo(dT) primer to generate single stranded cDNA followed by a second strand synthesis to generate double stranded cDNA which is then column purified. In vitro transcription with T7 RNA polymerase generated biotin-labeled cRNA. The cRNA was then column purified, checked for size and yield using the Bio-Rad Experion system, and then 1.5 μg of cRNA was hybridized to each array using standard Illumina protocols with streptavidin-Cy3 (Amersham) being used for detection. Slides were scanned and fluorescence intensity captured using an Illumina BeadStation. Expression values from were extracted using BeadStudio v3.3. The data was background subtracted and quantile-normalized using the MBCB algorithm (Allen et al., 2009; Ding et al., 2008; Xie et al., 2009). _miRNA expression profiling was conducted using an Illumina human v2 miRNA panel following manufacturer's protocols.

Clinical Outcomes and Associations

We downloaded and analyzed data publicly available from the Cancer Genome Atlas Project (TCGA; http://tcga-data.nci.nih.gov/) for patients with ovarian serous cystadenocarcinoma. Level 3 IlluminaHiSeq miRNASeq and Agilent MicroRNA microarray data were used for miRNA expression. For miRNASeq data we derived from the "isoform_quantification" files containing the "reads_per_million_miRNA_mapped" values for mature forms for each microRNA. Survival analyses were performed in R (version 2.14.2) and the statistical significance was defined as a p-value less 0.05. The Log-rank test was employed to determine the relationship between expression and overall survival and the Kaplan-Meier method was used to generate survival curves. We randomly split the entire population into training/validation cohorts (2/3, 1/3). For each miRNA, we checked for a relation with the survival as follows. In both cohorts, patients were divided into percentiles according to miRNA expression. Using the training set, we considered any cut-off between the 25th and 75th percentile that significantly split the samples and verified the statistical significance in the validation set.

For SIX4 expression analysis, we used the gene expression data run by UNC on Agilent Expression 244K microarrays measuring 17814 genes. The data involve 598 samples, of which 36 samples were run by one batch and the remaining 563 were run by the other batch. We performed principal component analysis (PCA) on the combined expression data and found no obvious batch effect (figure not shown). Of the 598 samples, 573 are primary solid tumors, 17

are recurrent solid tumors and 8 are normal solid tissue samples. We extracted the expression levels of SIX4 from all samples and generated a box plot. The data processing and statistical analyses were performed in R (R-Core-Team, 2012).

Cell Cycle and Growth Assays

For evaluation of caspase 3/7 activation in cells, we transfected cells as above except cells were plated in a total volume of 100 μL. After 48 hours, cells were incubated with 50 μL of CaspaseGlo 3/7 reagent (Promega) per manufacturer's protocol. Luminescence values were read on a PheraStar plate reader (BMG LabTech) and raw luminescence values were normalized to a negative control siRNA contained on each plate. BrdU incorporation assays were performed by incubating cells with 10 μM BrdU for 4 hours, 48-hours after transfection as described above. After incubation cells were fixed with 3.7% paraformaldehyde. DNA was denatured using 0.5N HCl and cells were stained with anti-BrdU antibody conjugated to Alexa-488 (Invitrogen) per manufacturer's instructions. Hoechst dye (Invitrogen) with then diluted in PBS per manufacturer's protocol and added to each well. Plates were read using a BD Pathway 855 microscope (BD Biosciences). Using AttoVision software (BD Biosciences), cells were segmented and Hoechst-positive and FITC-positive nuclei were automatically counted. Cutoffs to segregate positive nuclei were empirically determined and constant for the entire plate. DNA content analysis was performed 48-hours after transfection. Cells were stained with propidium iodide (PI) using a PI/RNase Buffer (BD Biosciences) following manufacturer's protocol.

Samples were run on a FACSCalibur flow cytometer and acquired with CellQuest Pro, (Becton Dickinson, San Jose, CA).

Samples were analyzed with Flowjo, (Treestar). Gating was performed to gate out dead cells and doublets and then Dean/Jet/Fox modeling was applied.

Drug Treatments and Western Blotting

Cells were plated and allowed to recover overnight before being treated with either LY294002 (Sigma) or AKT Inhibitor X (EMD Biosciences). After 48 hours, cells were lysed in boiling SDS-Tris to generate lysates for western blotting. For stimulation experiments, a similar protocol was followed but cells were stimulated with either 10% Fetal Bovine Serum (Atlanta Biologicals) or 10 ng/mL TGFβ1 (Cell Signaling)

CHAPTER THREE
Future Directions and Concluding Remarks

The work I have done has demonstrated the incredible functional diversity of ovarian cancer cells, which mirrors the previously reported genetic diversity of this disease. The multiplicity of genetic changes and functional vulnerabilities further emphasizes the need to move cancer treatment towards a goal of personalized therapy. Previously, cancer research focused on understanding the biology of cancer, with the ultimate goal of identifying an exploitable vulnerability common to all cancers. Such a vulnerability would allow for the discovery of a "silver bullet" treatment that would effectively cure all cancers. As our understanding of the genetic and molecular alterations underlying cancer progression has grown, it has become increasingly self-evident that likelihood of such a "silver bullet" existing is extremely improbable. In fact, it appears that most solid tumors exhibit breathtaking heterogeneity, and novel treatments will realistically be efficacious in only a small subset of tumors. In addition to creating challenges in treatment identification, the diversity observed in cancer also leads to a challenge of identifying the correct patient to be treated with the correct drug. Understanding the functional and genetic diversity of cancer then becomes imperative to push forward development of personalized therapies. The screen conducted here hopefully contributes to a greater understanding of ovarian tumors and will contribute to the generation of new treatments. The work I conducted also suggested that miRNA deregulation might play an important and common role in tumor progression. Alteration of miRNA expression might allow

tumors to deflect cell differentiation programs and maintain an undifferentiated state. I was able to show that restoration of expression of miRNAs can lead to re-engagement of differentiation programs with sometimes catastrophic consequences. More practically, I was also able to demonstrate that miRNA seed sequences can be used to predict functional targets and effects of miRNA expression. This ability could prove to be important to increasing our understanding of how miRNAs function in cells and uncovering mechanisms of miRNA actions in cells.

Moving forward, my project has brought up several questions that remain to be answered. miR-517a appeared to reduce ovarian cancer cell viability by inhibiting expression of ARCN1. This miRNA is not predicted to target any other members of the coatamer complex suggesting that ARCN1 is either a very sensitive regulatory node or that ARCN1 has some other function supporting ovarian cancer viability. More investigation into the mechanism by which ARCN1 expression supports ovarian cancer cell viability is required. One approach that might answer questions about the role ARCN1 is playing would be using an immunoprecipitation (IP) and mass spectrometry approach to identify interacting partners of ARCN1. Novel interactions might suggest novel functions for this gene in addition to vesicle trafficking in the cell. More importantly, interacting partners of ARCN1 might be druggable targets allowing for new pharmacologic interventions in ovarian cancer. miR-517a is also predicted to target USP1 and reduced expression of USP1. While USP1 depletion did not reduce cell viability in most ovarian lines, it did reduce viability in NSCLC lines. This selective toxicity needs to be further explored to determine the factors defining sensitivity to USP1 depletion. Additionally, another

deubiquitinase, USP7, has been shown to be a druggable target, so a screen could be conducted to identify inhibitors of USP1 (Chauhan et al., 2012; Reverdy et al., 2012). Combining an understanding of USP1 sensitivity and a pharmacologic inhibitor could lead to a new treatment for NSCLC and possibly some ovarian tumors.

SIX4 expression is increased in ovarian tumors and depletion of SIX4 expression reduced cell viability in multiple EOC cell lines. However, the consequences of SIX4 overexpression in ovarian cancer cells have yet to be explored. Functional cancer progression assays such as growth in soft agar, colony formation assays, and invasion assays could coarsely determine the effects of SIX4 overexpression. Chromatin immunoprecipitation followed by next generation sequencing (ChIP-Seq) could be used to explore the mechanisms of SIX4 action in cells. For instance, this approach could yield insight into whether SIX4 is directly leading to induction of cyclin protein expression or directly inhibiting STRADB expression. These approaches would yield a greater understanding of the biology underlying increased SIX4 expression in ovarian tumors, which might lead to identification of new drug targets.

Finally, the robust phenotypes observed upon miRNA overexpression suggest that these RNAs could be used therapeutically. Excitingly, the prospect of clinical delivery of miRNAs is appearing more and more likely. Recently, reports have demonstrated that single-stranded siRNAs (ss-siRNAs) could be shown to knockdown targets in an allele-specific manner and be delivered effectively in vivo (Gagnon et al., 2010; Hu et al., 2009; Yu et al., 2012). Furthermore, to achieve allele-specific targeting this group synthesized ss-siRNAs with mismatches, making

them function similarly to miRNAs (Hu et al., 2010). This data suggests that single-stranded miRNAs could be synthesized which would function in vivo. I have begun working with a company to synthesize single-stranded miRNA mimics. These mimics utilized locked nucleic acid (LNA) technology, which renders them resistant to RNases in vivo. These LNA mimics can also be modified for passive delivery allowing for administration without incorporation into liposomes. Pilot studies have demonstrated that these single-stranded mimics have efficacy in vitro and can recapitulate some of the selectivity of other mimics (Figure 3.1).

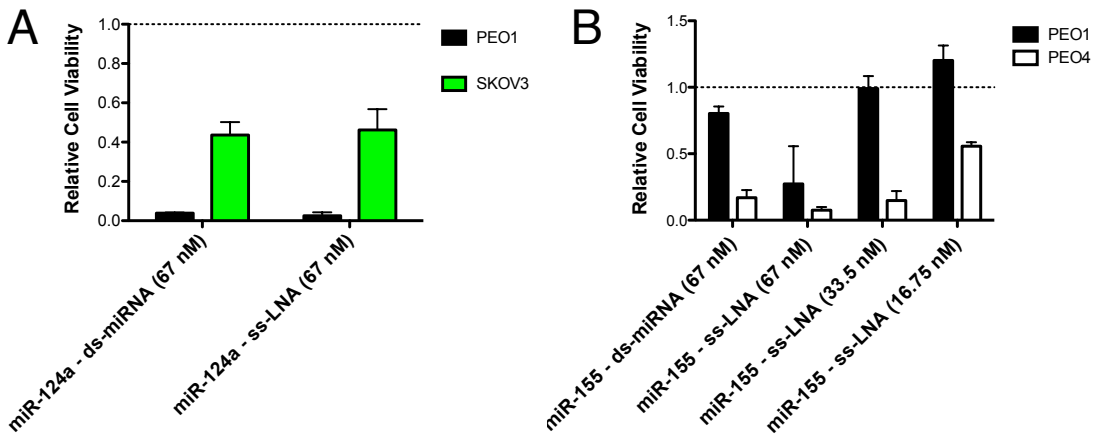

Figure 3.1 Single-stranded LNA mimics (ss-LNA) faithfully recapitulate the phenotype and selectivity of double-stranded mimics (ds-miRNA).

(A) A miR-124a ds-miRNA mimic from Dharmacon and a ss-LNA mimic reduced cell viability at similar levels in PEO1 and SKOV3 cells.

(B) Lower doses of a ss-LNA miR-155 mimic recapitulated the selective toxicity seen by a miR-155 ds-miRNA mimic from Dharmacon in PEO1 and PEO4.

These data suggest that these LNA mimics might be able to function in vivo and reduce ovarian cancer cell viability. Further work needs to be conducted to determine the specificity of these LNA mimics. In addition to controlling for chemistry effects, the ability to passively deliver these LNA mimics needs to be evaluated in vitro and in vivo. Studies can then be conducted to determine the efficacy of LNA mimics in vivo. miRNAs might even make more effective interventions than drugs. The multigenic nature of miRNA targeting has evolved in concert with cell processes to allow miRNAs to tightly regulate multiple nodes involved in a progress. Therefore, unlike a drug, a single miRNA is able to target multiple genes supporting cancer cell survival, perhaps reducing the possibility of resistance arising. Moreover, my work has demonstrated that expression of a single miRNA is sufficient to drive a cell differentiation program even in the complex genetic background of an ovarian caner cell. Therefore, miRNAs could perhaps be effective drugs to achieve differentiation therapy in cancers, driving differentiation of cancer cells halting tumor progression.

APPENDIX A
Supplementary Figures

A.

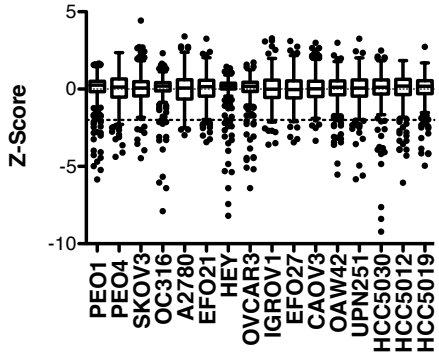

B.

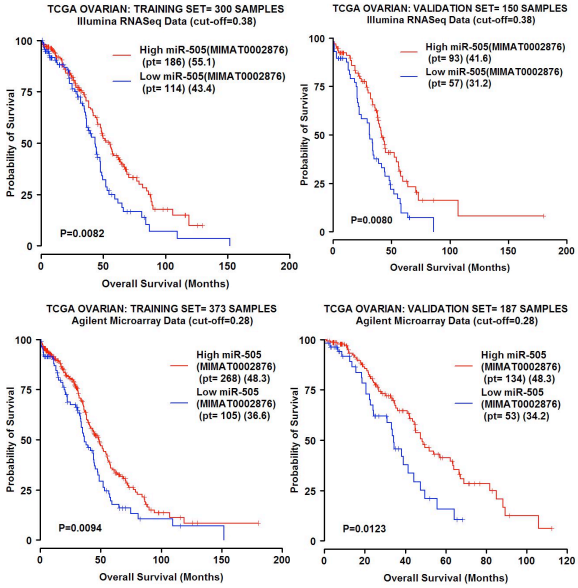

C.

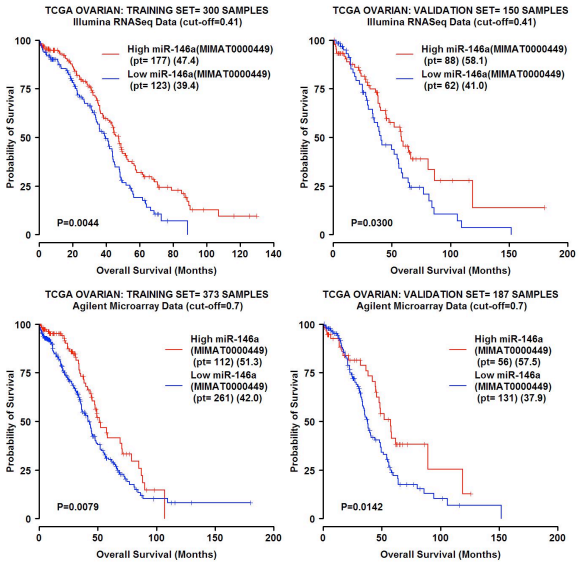

Figure A1.1 A miRNA mimic screen identified multiple miRNAs toxic to ovarian cancer cells and two that correlated with patient outcomes.

(A) A Tukey plot of the range of z-scores for all mimics screened in each cell line screened.

(B) Kaplan-Meier plots of training and validation sets of tumors using miRNA expression from both Agilent arrays and Illumina miRseq showed that higher expression of miR-505 correlated with increased patient survival.

(C) Kaplan-Meier plots of training and validation sets of tumors using miRNA expression from both Agilent arrays and Illumina miRseq showed that higher expression of miR-146a correlated with increased patient survival.

A

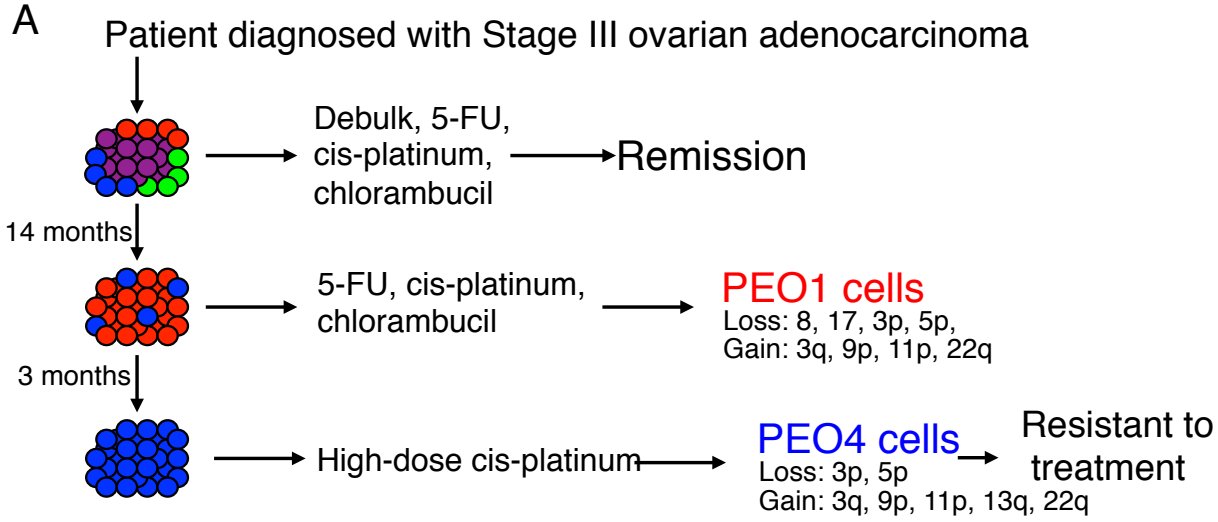
Patient diagnosed with Stage III ovarian adenocarcinoma
Debulk, 5-FU, cis-platinum, chlorambucil
Remission
14 months
5-FU, cis-platinum, chlorambucil
PEO1 cells
Loss: 8, 17, 3p, 5p,
Gain: 3q, 9p, 11p, 22q
3 months
High-dose cis-platinum
PEO4 cells
Loss: 3p, 5p
Gain: 3q, 9p, 11p, 13q, 22q
Resistant to treatment

B

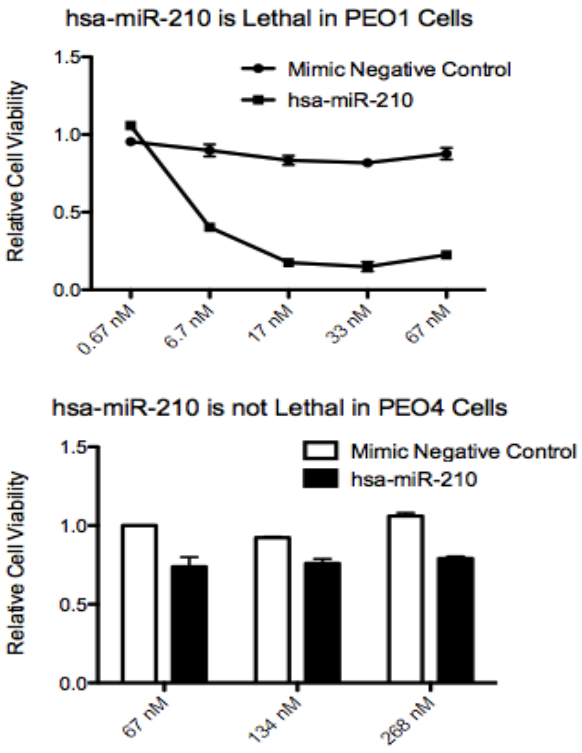
hsa-miR-210 is Lethal in PEO1 Cells
Mimic Negative Control
hsa-miR-210
Relative Cell Viability
1.5
1.0
0.5
0.0
0.67 nM
6.7 nM
17 nM
33 nM
67 nM
hsa-miR-210 is not Lethal in PEO4 Cells
Mimic Negative Control
hsa-miR-210
Relative Cell Viability
1.5
1.0
0.5
0.0
67 nM
134 nM
268 nM

Figure A1.2 Specific hits are not dosage driven.

(A) A cartoon depicting the derivation of the PEO1 and PEO4 cell lines from a patient with high-grade serous adenocarcinoma of the ovary.

(B) PEO1-specific hit miR-210 continues to show a robust phenotype at even a 10-fold dilution while increasing the dosage 4-fold does not sensitize PEO4 cells, suggesting that the phenotype observed was not due to dosage effects.

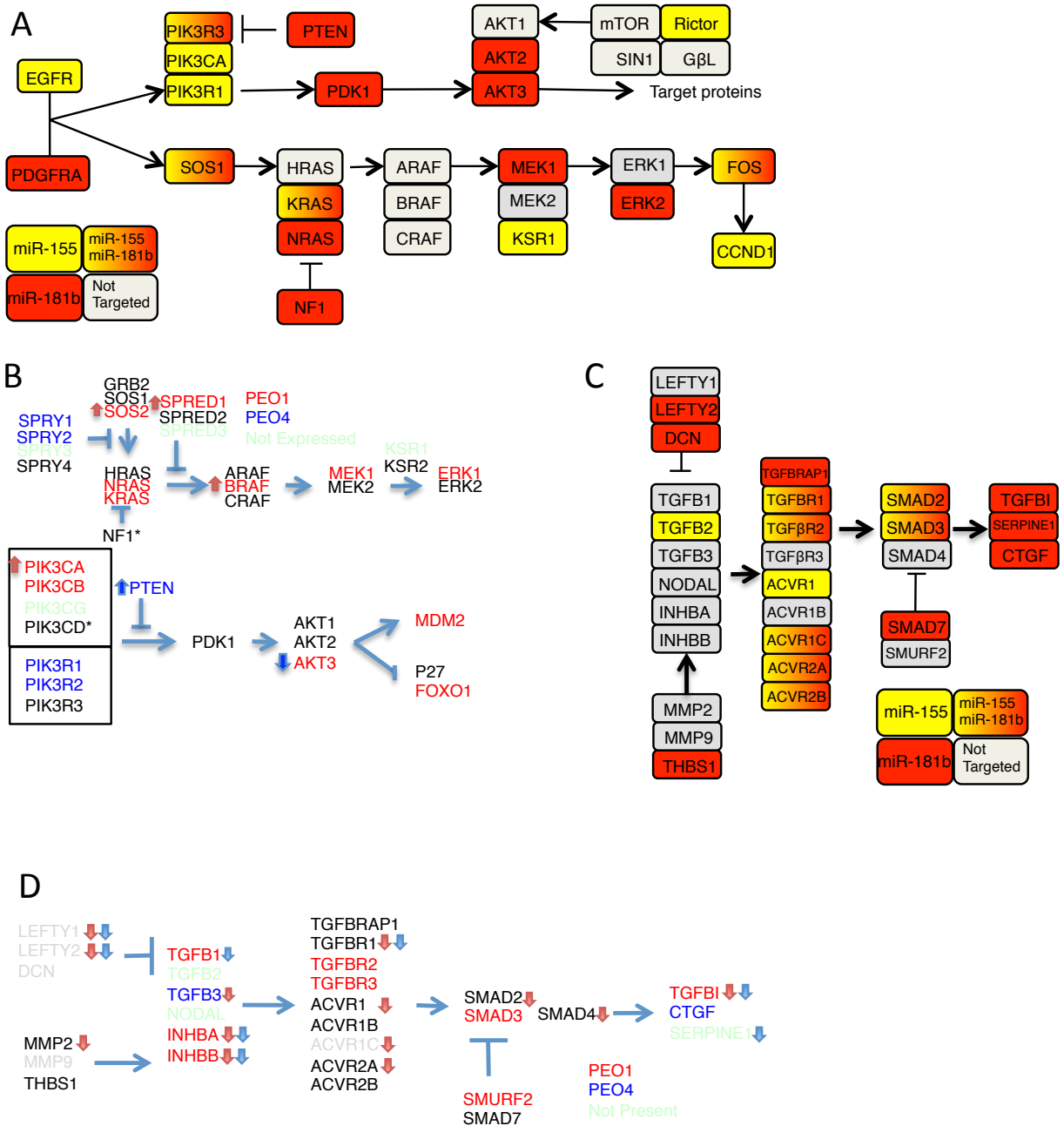
A
EGFR
PDGFRA
PIK3R3
PIK3CA
PIK3R1
PTEN
PDK1
AKT1
AKT2
AKT3
mTOR
Rictor
SIN1
GβL
Target proteins
SOS1
HRAS
KRAS
NRAS
NF1
ARAF
BRAF
CRAF
MEK1
MEK2
KSR1
ERK1
ERK2
FOS
CCND1
miR-155
miR-155
miR-181b
miR-181b
Not Targeted
B
GRB2
SOS1
SOS2
SPRED1
SPRED2
SPRED3
PEO1
PEO4
Not Expressed
SPRY1
SPRY2
SPRY3
SPRY4
HRAS
NRAS
KRAS
NF1*
ARAF
BRAF
CRAF
MEK1
MEK2
KSR1
KSR2
ERK1
ERK2
PIK3CA
PIK3CB
PIK3CG
PIK3CD*
PIK3R1
PIK3R2
PIK3R3
PTEN
PDK1
AKT1
AKT2
AKT3
MDM2
P27
FOXO1
C
LEFTY1
LEFTY2
DCN
TGFB1
TGFB2
TGFB3
NODAL
INHBA
INHBB
MMP2
MMP9
THBS1
TGFBRAP1
TGFBR1
TGFβR2
TGFβR3
ACVR1
ACVR1B
ACVR1C
ACVR2A
ACVR2B
SMAD2
SMAD3
SMAD4
SMAD7
SMURF2
TGFBI
SERPINE1
CTGF
miR-155
miR-155
miR-181b
miR-181b
Not Targeted
D
LEFTY1
LEFTY2
DCN
TGFB1
TGFB2
TGFB3
NODAL
INHBA
INHBB
MMP2
MMP9
THBS1
TGFBRAP1
TGFBR1
TGFBR2
TGFBR3
ACVR1
ACVR1B
ACVR1C
ACVR2A
ACVR2B
SMAD2
SMAD3
SMAD4
SMURF2
SMAD7
TGFBI
CTGF
SERPINE1
PEO1
PEO4
Not Present

Figure A1.3 miR-155 and miR-181b are predicted to target the AKT, MAPK, and TGFβ pathways.

(A) miR-155 and miR-181b are predicted to target multiple nodes in the AKT and MAPK signaling pathways. Nodes predicted to be targeted by miR-155 are in yellow, miR-181b in red, those predicted to be targeted by both are in yellow-to-red gradient, and those predicted to be target by neither are in gray. Notice only miR-155 is predicted to target Rictor, which is part of the complex responsible for phosphorylation of AKT at S473.

(B) High-resolution genomic data predicted differences in signaling of the AKT and MAPK pathways in PEO1 and PEO4 cells. Genes in red were overexpressed at least 2-fold in PEO1 relative to PEO4 cells, while genes in blue were overexpressed in PEO4 relative to PEO1. Arrows indicated copy gain or loss with red indicating PEO1 cells and blue indicating PEO4. Asterisks denote genes containing SNVs.

(C) miR-155 and miR-181b are predicted to target multiple nodes in the TGFβ signaling pathway. Nodes predicted to be targeted by miR-155 are in yellow, miR-181b in red, those predicted to be targeted by both are in yellow-to-red gradient, and those predicted to be target by neither are in gray.

(D) High-resolution genomic data predicted differences in signaling of the TGFβ pathway in PEO1 and PEO4 cells. Genes in red were overexpressed at least 2-fold in PEO1 relative to PEO4 cells, while genes in blue were overexpressed in PEO4 relative to PEO1. Arrows indicate

copy gain or loss with red indicating PEO1 cells and blue indicating PEO4. Asterisks denote genes containing SNVs.

REFERENCES

Agirre, X., Vilas-Zornoza, A., Jimenez-Velasco, A., Martin-Subero, J. I., Cordeu, L., Garate, L., San Jose-Eneriz, E., Abizanda, G., Rodriguez-Otero, P., Fortes, P.*, et al.* (2009). Epigenetic silencing of the tumor suppressor microRNA Hsa-miR-124a regulates CDK6 expression and confers a poor prognosis in acute lymphoblastic leukemia. Cancer Res *69*, 4443-4453.

Ahmed, A. A., Etemadmoghadam, D., Temple, J., Lynch, A. G., Riad, M., Sharma, R., Stewart, C., Fereday, S., Caldas, C., Defazio, A.*, et al.* (2010). Driver mutations in TP53 are ubiquitous in high grade serous carcinoma of the ovary. The Journal of pathology *221*, 49-56.

Aletti, G. D., Dowdy, S. C., Gostout, B. S., Jones, M. B., Stanhope, C. R., Wilson, T. O., Podratz, K. C., and Cliby, W. A. (2006). Aggressive surgical effort and improved survival in advanced-stage ovarian cancer. Obstetrics and gynecology *107*, 77-85.

Allen, J. D., Chen, M., and Xie, Y. (2009). Model-Based Background Correction (MBCB): R Methods and GUI for Illumina Bead-array Data. J Cancer Sci Ther *1*, 25-27.

Armstrong, D. K., Bundy, B., Wenzel, L., Huang, H. Q., Baergen, R., Lele, S., Copeland, L. J., Walker, J. L., and Burger, R. A. (2006). Intraperitoneal cisplatin and paclitaxel in ovarian cancer. N Engl J Med *354*, 34-43.

Ayhan, A., Mao, T. L., Seckin, T., Wu, C. H., Guan, B., Ogawa, H., Futagami, M., Mizukami, H., Yokoyama, Y., Kurman, R. J., and Shih Ie, M. (2012). Loss of ARID1A expression is an

early molecular event in tumor progression from ovarian endometriotic cyst to clear cell and endometrioid carcinoma. International journal of gynecological cancer : official journal of the International Gynecological Cancer Society *22*, 1310-1315.

Bartel, D. P. (2009). MicroRNAs: target recognition and regulatory functions. Cell *136*, 215-233.

Bast, R. C., Jr., Hennessy, B., and Mills, G. B. (2009). The biology of ovarian cancer: new opportunities for translation. Nat Rev Cancer *9*, 415-428.

Bowtell, D. D. (2010). The genesis and evolution of high-grade serous ovarian cancer. Nat Rev Cancer *10*, 803-808.

Byers, L. A., Diao, L., Wang, J., Saintigny, P., Girard, L., Peyton, M., Shen, L., Fan, Y., Giri, U., Tumula, P. K.*, et al.* (2013). An epithelial-mesenchymal transition gene signature predicts resistance to EGFR and PI3K inhibitors and identifies Axl as a therapeutic target for overcoming EGFR inhibitor resistance. Clinical cancer research : an official journal of the American Association for Cancer Research *19*, 279-290.

Calin, G. A., Liu, C. G., Sevignani, C., Ferracin, M., Felli, N., Dumitru, C. D., Shimizu, M., Cimmino, A., Zupo, S., Dono, M.*, et al.* (2004). MicroRNA profiling reveals distinct signatures in B cell chronic lymphocytic leukemias. Proc Natl Acad Sci U S A *101*, 11755-11760.

Cancer Genome Atlas Research, N. (2011). Integrated genomic analyses of ovarian carcinoma. Nature *474*, 609-615.

Chauhan, D., Tian, Z., Nicholson, B., Kumar, K. G., Zhou, B., Carrasco, R., McDermott, J. L., Leach, C. A., Fulcinniti, M., Kodrasov, M. P.*, et al.* (2012). A small molecule inhibitor of ubiquitin-specific protease-7 induces apoptosis in multiple myeloma cells and overcomes bortezomib resistance. Cancer cell *22*, 345-358.

Chen, C. Z., Li, L., Lodish, H. F., and Bartel, D. P. (2004). MicroRNAs modulate hematopoietic lineage differentiation. Science *303*, 83-86.

Chen, G., Umelo, I. A., Lv, S., Teugels, E., Fostier, K., Kronenberger, P., Dewaele, A., Sadones, J., Geers, C., and De Greve, J. (2013). miR-146a Inhibits Cell Growth, Cell Migration and Induces Apoptosis in Non-Small Cell Lung Cancer Cells. PloS one *8*, e60317.

Cheung, H. W., Cowley, G. S., Weir, B. A., Boehm, J. S., Rusin, S., Scott, J. A., East, A., Ali, L. D., Lizotte, P. H., Wong, T. C.*, et al.* (2011). Systematic investigation of genetic vulnerabilities across cancer cell lines reveals lineage-specific dependencies in ovarian cancer. Proc Natl Acad Sci U S A *108*, 12372-12377.

Cittelly, D. M., Dimitrova, I., Howe, E. N., Cochrane, D. R., Jean, A., Spoelstra, N. S., Post, M. D., Lu, X., Broaddus, R. R., Spillman, M. A., and Richer, J. K. (2012). Restoration of miR-200c to ovarian cancer reduces tumor burden and increases sensitivity to paclitaxel. Molecular cancer therapeutics *11*, 2556-2565.

Cooke, S. L., Ng, C. K., Melnyk, N., Garcia, M. J., Hardcastle, T., Temple, J., Langdon, S., Huntsman, D., and Brenton, J. D. (2010). Genomic analysis of genetic heterogeneity and evolution in high-grade serous ovarian carcinoma. Oncogene *29*, 4905-4913.

Costinean, S., Zanesi, N., Pekarsky, Y., Tili, E., Volinia, S., Heerema, N., and Croce, C. M. (2006). Pre-B cell proliferation and lymphoblastic leukemia/high-grade lymphoma in E(mu)-miR155 transgenic mice. Proc Natl Acad Sci U S A *103*, 7024-7029.

Creighton, C. J., Hernandez-Herrera, A., Jacobsen, A., Levine, D. A., Mankoo, P., Schultz, N., Du, Y., Zhang, Y., Larsson, E., Sheridan, R.*, et al.* (2012). Integrated analyses of microRNAs demonstrate their widespread influence on gene expression in high-grade serous ovarian carcinoma. PloS one *7*, e34546.

Dahiya, N., Sherman-Baust, C. A., Wang, T. L., Davidson, B., Shih Ie, M., Zhang, Y., Wood, W., 3rd, Becker, K. G., and Morin, P. J. (2008). MicroRNA expression and identification of putative miRNA targets in ovarian cancer. PloS one *3*, e2436.

Davalos, V., Moutinho, C., Villanueva, A., Boque, R., Silva, P., Carneiro, F., and Esteller, M. (2012). Dynamic epigenetic regulation of the microRNA-200 family mediates epithelial and mesenchymal transitions in human tumorigenesis. Oncogene *31*, 2062-2074.

de The, H., Chomienne, C., Lanotte, M., Degos, L., and Dejean, A. (1990). The t(15;17) translocation of acute promyelocytic leukaemia fuses the retinoic acid receptor alpha gene to a novel transcribed locus. Nature *347*, 558-561.

Ding, L. H., Xie, Y., Park, S., Xiao, G., and Story, M. D. (2008). Enhanced identification and biological validation of differential gene expression via Illumina whole-genome expression arrays through the use of the model-based background correction methodology. Nucleic Acids Res *36*, e58.

Eis, P. S., Tam, W., Sun, L., Chadburn, A., Li, Z., Gomez, M. F., Lund, E., and Dahlberg, J. E. (2005). Accumulation of miR-155 and BIC RNA in human B cell lymphomas. Proc Natl Acad Sci U S A *102*, 3627-3632.

Eisenkop, S. M., Spirtos, N. M., Friedman, R. L., Lin, W. C., Pisani, A. L., and Perticucci, S. (2003). Relative influences of tumor volume before surgery and the cytoreductive outcome on survival for patients with advanced ovarian cancer: a prospective study. Gynecol Oncol *90*, 390-396.

Etemadmoghadam, D., deFazio, A., Beroukhim, R., Mermel, C., George, J., Getz, G., Tothill, R., Okamoto, A., Raeder, M. B., Harnett, P.*, et al.* (2009). Integrated genome-wide DNA copy number and expression analysis identifies distinct mechanisms of primary chemoresistance in ovarian carcinomas. Clinical cancer research : an official journal of the American Association for Cancer Research *15*, 1417-1427.

Flesken-Nikitin, A., Hwang, C. I., Cheng, C. Y., Michurina, T. V., Enikolopov, G., and Nikitin, A. Y. (2013). Ovarian surface epithelium at the junction area contains a cancer-prone stem cell niche. Nature *495*, 241-245.

Folkins, A. K., Jarboe, E. A., Roh, M. H., and Crum, C. P. (2009). Precursors to pelvic serous carcinoma and their clinical implications. Gynecol Oncol *113*, 391-396.

Gagnon, K. T., Pendergraff, H. M., Deleavey, G. F., Swayze, E. E., Potier, P., Randolph, J., Roesch, E. B., Chattopadhyaya, J., Damha, M. J., Bennett, C. F.*, et al.* (2010). Allele-selective inhibition of mutant huntingtin expression with antisense oligonucleotides targeting the expanded CAG repeat. Biochemistry *49*, 10166-10178.

Ganesan, A. K., Ho, H., Bodemann, B., Petersen, S., Aruri, J., Koshy, S., Richardson, Z., Le, L. Q., Krasieva, T., Roth, M. G.*, et al.* (2008). Genome-wide siRNA-based functional genomics of pigmentation identifies novel genes and pathways that impact melanogenesis in human cells. PLoS Genet *4*, e1000298.

Garcia, A. I., Buisson, M., Bertrand, P., Rimokh, R., Rouleau, E., Lopez, B. S., Lidereau, R., Mikaelian, I., and Mazoyer, S. (2011a). Down-regulation of BRCA1 expression by miR-146a and miR-146b-5p in triple negative sporadic breast cancers. EMBO molecular medicine *3*, 279-290.

Garcia, A. I., Cox, D. G., Barjhoux, L., Verny-Pierre, C., Barnes, D., Gemo Study, C., Antoniou, A. C., Stoppa-Lyonnet, D., Sinilnikova, O. M., and Mazoyer, S. (2011b). The rs2910164:G>C SNP in the MIR146A gene is not associated with breast cancer risk in BRCA1 and BRCA2 mutation carriers. Human mutation.

Goff, B. A., Mandel, L., Muntz, H. G., and Melancon, C. H. (2000). Ovarian carcinoma diagnosis. Cancer *89*, 2068-2075.

Gregory, P. A., Bert, A. G., Paterson, E. L., Barry, S. C., Tsykin, A., Farshid, G., Vadas, M. A., Khew-Goodall, Y., and Goodall, G. J. (2008). The miR-200 family and miR-205 regulate epithelial to mesenchymal transition by targeting ZEB1 and SIP1. Nature cell biology *10*, 593-601.

Grishok, A., Pasquinelli, A. E., Conte, D., Li, N., Parrish, S., Ha, I., Baillie, D. L., Fire, A., Ruvkun, G., and Mello, C. C. (2001). Genes and mechanisms related to RNA interference regulate expression of the small temporal RNAs that control C. elegans developmental timing. Cell *106*, 23-34.

Guan, B., Wang, T. L., and Shih Ie, M. (2011). ARID1A, a factor that promotes formation of SWI/SNF-mediated chromatin remodeling, is a tumor suppressor in gynecologic cancers. Cancer Res *71*, 6718-6727.

Hanrahan, A. J., Schultz, N., Westfal, M. L., Sakr, R. A., Giri, D. D., Scarperi, S., Janakiraman, M., Olvera, N., Stevens, E. V., She, Q. B.*, et al.* (2012). Genomic complexity and AKT dependence in serous ovarian cancer. Cancer discovery *2*, 56-67.

Hatley, M. E., Patrick, D. M., Garcia, M. R., Richardson, J. A., Bassel-Duby, R., van Rooij, E., and Olson, E. N. (2010). Modulation of K-Ras-dependent lung tumorigenesis by MicroRNA-21. Cancer cell *18*, 282-293.

Holleman, A., Chung, I., Olsen, R. R., Kwak, B., Mizokami, A., Saijo, N., Parissenti, A., Duan, Z., Voest, E. E., and Zetter, B. R. (2011). miR-135a contributes to paclitaxel resistance in tumor cells both in vitro and in vivo. Oncogene *30*, 4386-4398.

Howlander N, N. A., Krapcho M, Neyman N, Aminou R, Altekruse SF, Kosary CL, Ruhl J, Tatalovich Z, Cho H, Mariotto A, Eisner MP, Lewis DR, Chen HS, Feuer EJ, Cronin KA (2012). SEER Cancer Statistics Review, 1975-2009 (Vintage 2009 Populations). In, (Bethesda, MD: National Cancer Institute).

Hu, J., Liu, J., and Corey, D. R. (2010). Allele-selective inhibition of huntingtin expression by switching to an miRNA-like RNAi mechanism. Chemistry & biology *17*, 1183-1188.

Hu, J., Matsui, M., and Corey, D. R. (2009). Allele-selective inhibition of mutant huntingtin by peptide nucleic acid-peptide conjugates, locked nucleic acid, and small interfering RNA. Annals of the New York Academy of Sciences *1175*, 24-31.

Hutvagner, G., McLachlan, J., Pasquinelli, A. E., Balint, E., Tuschl, T., and Zamore, P. D. (2001). A cellular function for the RNA-interference enzyme Dicer in the maturation of the let-7 small temporal RNA. Science *293*, 834-838.

Hutvagner, G., and Zamore, P. D. (2002). A microRNA in a multiple-turnover RNAi enzyme complex. Science *297*, 2056-2060.

Iorio, M. V., Visone, R., Di Leva, G., Donati, V., Petrocca, F., Casalini, P., Taccioli, C., Volinia, S., Liu, C. G., Alder, H.*, et al.* (2007). MicroRNA signatures in human ovarian cancer. Cancer Res *67*, 8699-8707.

Jarboe, E. A., Folkins, A. K., Drapkin, R., Ince, T. A., Agoston, E. S., and Crum, C. P. (2008). Tubal and ovarian pathways to pelvic epithelial cancer: a pathological perspective. Histopathology *53*, 127-138.

Jazdzewski, K., Murray, E. L., Franssila, K., Jarzab, B., Schoenberg, D. R., and de la Chapelle, A. (2008). Common SNP in pre-miR-146a decreases mature miR expression and predisposes to papillary thyroid carcinoma. Proc Natl Acad Sci U S A *105*, 7269-7274.

Johnson, S. M., Lin, S. Y., and Slack, F. J. (2003). The time of appearance of the C. elegans let-7 microRNA is transcriptionally controlled utilizing a temporal regulatory element in its promoter. Developmental biology *259*, 364-379.

Johnston, R. J., and Hobert, O. (2003). A microRNA controlling left/right neuronal asymmetry in Caenorhabditis elegans. Nature *426*, 845-849.

Jones, S., Wang, T. L., Shih Ie, M., Mao, T. L., Nakayama, K., Roden, R., Glas, R., Slamon, D., Diaz, L. A., Jr., Vogelstein, B.*, et al.* (2010). Frequent mutations of chromatin remodeling gene ARID1A in ovarian clear cell carcinoma. Science *330*, 228-231.

Kan, Z., Jaiswal, B. S., Stinson, J., Janakiraman, V., Bhatt, D., Stern, H. M., Yue, P., Haverty, P. M., Bourgon, R., Zheng, J.*, et al.* (2010). Diverse somatic mutation patterns and pathway alterations in human cancers. Nature *466*, 869-873.

Kelemen, L. E., and Kobel, M. (2011). Mucinous carcinomas of the ovary and colorectum: different organ, same dilemma. The lancet oncology *12*, 1071-1080.

Ketting, R. F., Fischer, S. E., Bernstein, E., Sijen, T., Hannon, G. J., and Plasterk, R. H. (2001). Dicer functions in RNA interference and in synthesis of small RNA involved in developmental timing in C. elegans. Genes & development *15*, 2654-2659.

Kim, J., Coffey, D. M., Creighton, C. J., Yu, Z., Hawkins, S. M., and Matzuk, M. M. (2012). High-grade serous ovarian cancer arises from fallopian tube in a mouse model. Proc Natl Acad Sci U S A *109*, 3921-3926.

Kindelberger, D. W., Lee, Y., Miron, A., Hirsch, M. S., Feltmate, C., Medeiros, F., Callahan, M. J., Garner, E. O., Gordon, R. W., Birch, C.*, et al.* (2007). Intraepithelial carcinoma of the fimbria

and pelvic serous carcinoma: Evidence for a causal relationship. The American journal of surgical pathology *31*, 161-169.

Korpal, M., Lee, E. S., Hu, G., and Kang, Y. (2008). The miR-200 family inhibits epithelial-mesenchymal transition and cancer cell migration by direct targeting of E-cadherin transcriptional repressors ZEB1 and ZEB2. J Biol Chem *283*, 14910-14914.

Kumar, M. S., Pester, R. E., Chen, C. Y., Lane, K., Chin, C., Lu, J., Kirsch, D. G., Golub, T. R., and Jacks, T. (2009). Dicer1 functions as a haploinsufficient tumor suppressor. Genes & development *23*, 2700-2704.

Lagos-Quintana, M., Rauhut, R., Lendeckel, W., and Tuschl, T. (2001). Identification of novel genes coding for small expressed RNAs. Science *294*, 853-858.

Lancaster, J. M., Wooster, R., Mangion, J., Phelan, C. M., Cochran, C., Gumbs, C., Seal, S., Barfoot, R., Collins, N., Bignell, G.*, et al.* (1996). BRCA2 mutations in primary breast and ovarian cancers. Nature genetics *13*, 238-240.

Landen, C. N., Jr., Chavez-Reyes, A., Bucana, C., Schmandt, R., Deavers, M. T., Lopez-Berestein, G., and Sood, A. K. (2005). Therapeutic EphA2 gene targeting in vivo using neutral liposomal small interfering RNA delivery. Cancer Res *65*, 6910-6918.

Landgraf, P., Rusu, M., Sheridan, R., Sewer, A., Iovino, N., Aravin, A., Pfeffer, S., Rice, A., Kamphorst, A. O., Landthaler, M*., et al.* (2007). A mammalian microRNA expression atlas based on small RNA library sequencing. Cell *129*, 1401-1414.

Larson, R. A., Kondo, K., Vardiman, J. W., Butler, A. E., Golomb, H. M., and Rowley, J. D. (1984). Evidence for a 15;17 translocation in every patient with acute promyelocytic leukemia. The American journal of medicine *76*, 827-841.

Lau, N. C., Lim, L. P., Weinstein, E. G., and Bartel, D. P. (2001). An abundant class of tiny RNAs with probable regulatory roles in Caenorhabditis elegans. Science *294*, 858-862.

Lee, Y., Ahn, C., Han, J., Choi, H., Kim, J., Yim, J., Lee, J., Provost, P., Radmark, O., Kim, S., and Kim, V. N. (2003). The nuclear RNase III Drosha initiates microRNA processing. Nature *425*, 415-419.

Lee, Y., Jeon, K., Lee, J. T., Kim, S., and Kim, V. N. (2002). MicroRNA maturation: stepwise processing and subcellular localization. The EMBO journal *21*, 4663-4670.

Levanon, K., Ng, V., Piao, H. Y., Zhang, Y., Chang, M. C., Roh, M. H., Kindelberger, D. W., Hirsch, M. S., Crum, C. P., Marto, J. A., and Drapkin, R. (2010). Primary ex vivo cultures of human fallopian tube epithelium as a model for serous ovarian carcinogenesis. Oncogene *29*, 1103-1113.

Levin, P. B. a. B. (2008). World Cancer Report 2008, (Lyon, France: International Agency for Research on Cancer).

Lewis, B. P., Burge, C. B., and Bartel, D. P. (2005). Conserved seed pairing, often flanked by adenosines, indicates that thousands of human genes are microRNA targets. Cell *120*, 15-20.

Lewis, B. P., Shih, I. H., Jones-Rhoades, M. W., Bartel, D. P., and Burge, C. B. (2003). Prediction of mammalian microRNA targets. Cell *115*, 787-798.

Li, X., Xu, B., Moran, M. S., Zhao, Y., Su, P., Haffty, B. G., Shao, C., and Yang, Q. (2012). 53BP1 functions as a tumor suppressor in breast cancer via the inhibition of NF-kappaB through miR-146a. Carcinogenesis *33*, 2593-2600.

Lim, L. P., Lau, N. C., Garrett-Engele, P., Grimson, A., Schelter, J. M., Castle, J., Bartel, D. P., Linsley, P. S., and Johnson, J. M. (2005). Microarray analysis shows that some microRNAs downregulate large numbers of target mRNAs. Nature *433*, 769-773.

Lindenblatt, C., Schulze-Osthoff, K., and Totzke, G. (2009). IkappaBzeta expression is regulated by miR-124a. Cell cycle *8*, 2019-2023.

Liu, R. F., Xu, X., Huang, J., Fei, Q. L., Chen, F., Li, Y. D., and Han, Z. G. (2013). Down-regulation of miR-517a and miR-517c promotes proliferation of hepatocellular carcinoma cells via targeting Pyk2. Cancer letters *329*, 164-173.

Liu, Y., Chu, A., Chakroun, I., Islam, U., and Blais, A. (2010). Cooperation between myogenic regulatory factors and SIX family transcription factors is important for myoblast differentiation. Nucleic acids research *38*, 6857-6871.

Lu, J., Getz, G., Miska, E. A., Alvarez-Saavedra, E., Lamb, J., Peck, D., Sweet-Cordero, A., Ebert, B. L., Mak, R. H., Ferrando, A. A.*, et al.* (2005). MicroRNA expression profiles classify human cancers. Nature *435*, 834-838.

Lu, T. P., Lee, C. Y., Tsai, M. H., Chiu, Y. C., Hsiao, C. K., Lai, L. C., and Chuang, E. Y. (2012). miRSystem: an integrated system for characterizing enriched functions and pathways of microRNA targets. PloS one *7*, e42390.

Lund, E., Guttinger, S., Calado, A., Dahlberg, J. E., and Kutay, U. (2004). Nuclear export of microRNA precursors. Science *303*, 95-98.

Mayr, C., and Bartel, D. P. (2009). Widespread shortening of 3'UTRs by alternative cleavage and polyadenylation activates oncogenes in cancer cells. Cell *138*, 673-684.

Merritt, W. M., Lin, Y. G., Han, L. Y., Kamat, A. A., Spannuth, W. A., Schmandt, R., Urbauer, D., Pennacchio, L. A., Cheng, J. F., Nick, A. M.*, et al.* (2008). Dicer, Drosha, and outcomes in patients with ovarian cancer. N Engl J Med *359*, 2641-2650.

Morales-Prieto, D. M., Chaiwangyen, W., Ospina-Prieto, S., Schneider, U., Herrmann, J., Gruhn, B., and Markert, U. R. (2012). MicroRNA expression profiles of trophoblastic cells. Placenta *33*, 725-734.

Mourelatos, Z., Dostie, J., Paushkin, S., Sharma, A., Charroux, B., Abel, L., Rappsilber, J., Mann, M., and Dreyfuss, G. (2002). miRNPs: a novel class of ribonucleoproteins containing numerous microRNAs. Genes & development *16*, 720-728.

Nam, Y. J., Song, K., Luo, X., Daniel, E., Lambeth, K., West, K., Hill, J. A., Dimaio, J. M., Baker, L. A., Bassel-Duby, R., and Olson, E. N. (2013). Reprogramming of human fibroblasts toward a cardiac fate. Proc Natl Acad Sci U S A *110*, 5588-5593.

Niro, C., Demignon, J., Vincent, S., Liu, Y., Giordani, J., Sgarioto, N., Favier, M., Guillet-Deniau, I., Blais, A., and Maire, P. (2010). Six1 and Six4 gene expression is necessary to activate the fast-type muscle gene program in the mouse primary myotome. Developmental biology *338*, 168-182.

Ohto, H., Kamada, S., Tago, K., Tominaga, S. I., Ozaki, H., Sato, S., and Kawakami, K. (1999). Cooperation of six and eya in activation of their target genes through nuclear translocation of Eya. Molecular and cellular biology *19*, 6815-6824.

Papadopoulos, G. L., Alexiou, P., Maragkakis, M., Reczko, M., and Hatzigeorgiou, A. G. (2009). DIANA-mirPath: Integrating human and mouse microRNAs in pathways. Bioinformatics *25*, 1991-1993.

Park, S. M., Gaur, A. B., Lengyel, E., and Peter, M. E. (2008). The miR-200 family determines the epithelial phenotype of cancer cells by targeting the E-cadherin repressors ZEB1 and ZEB2. Genes & development *22*, 894-907.

Pastrello, C., Polesel, J., Della Puppa, L., Viel, A., and Maestro, R. (2010). Association between hsa-mir-146a genotype and tumor age-of-onset in BRCA1/BRCA2-negative familial breast and ovarian cancer patients. Carcinogenesis *31*, 2124-2126.

Pierson, J., Hostager, B., Fan, R., and Vibhakar, R. (2008). Regulation of cyclin dependent kinase 6 by microRNA 124 in medulloblastoma. Journal of neuro-oncology *90*, 1-7.

R-Core-Team (2012). R: A language and environment for statistical computing, (Vienna, Austria: R Foundation for Statistical Computing).

Reverdy, C., Conrath, S., Lopez, R., Planquette, C., Atmanene, C., Collura, V., Harpon, J., Battaglia, V., Vivat, V., Sippl, W., and Colland, F. (2012). Discovery of specific inhibitors of human USP7/HAUSP deubiquitinating enzyme. Chemistry & biology *19*, 467-477.

Rosen, D. G., Mercado-Uribe, I., Yang, G., Bast, R. C., Jr., Amin, H. M., Lai, R., and Liu, J. (2006). The role of constitutively active signal transducer and activator of transcription 3 in ovarian tumorigenesis and prognosis. Cancer *107*, 2730-2740.

Rubin, S. C., Blackwood, M. A., Bandera, C., Behbakht, K., Benjamin, I., Rebbeck, T. R., and Boyd, J. (1998). BRCA1, BRCA2, and hereditary nonpolyposis colorectal cancer gene mutations in an unselected ovarian cancer population: relationship to family history and implications for genetic testing. American journal of obstetrics and gynecology *178*, 670-677.

Shen, J., Ambrosone, C. B., DiCioccio, R. A., Odunsi, K., Lele, S. B., and Zhao, H. (2008). A functional polymorphism in the miR-146a gene and age of familial breast/ovarian cancer diagnosis. Carcinogenesis *29*, 1963-1966.

Shih, K. K., Qin, L. X., Tanner, E. J., Zhou, Q., Bisogna, M., Dao, F., Olvera, N., Viale, A., Barakat, R. R., and Levine, D. A. (2011). A microRNA survival signature (MiSS) for advanced ovarian cancer. Gynecol Oncol *121*, 444-450.

Siegel, R., Naishadham, D., and Jemal, A. (2012). Cancer statistics, 2012. CA: a cancer journal for clinicians *62*, 10-29.

Singh, N. K., Seo, B. Y., Vidyasagar, M., White, M. A., and Kim, H. S. (2013). siMacro: A Fast and Easy Data Processing Tool for Cell-Based Genomewide siRNA Screens. Genomics & informatics *11*, 55-57.

Small, E. M., O'Rourke, J. R., Moresi, V., Sutherland, L. B., McAnally, J., Gerard, R. D., Richardson, J. A., and Olson, E. N. (2010). Regulation of PI3-kinase/Akt signaling by muscle-enriched microRNA-486. Proc Natl Acad Sci U S A *107*, 4218-4223.

Storms, A. A., Sukumvanich, P., Monaco, S. E., Beriwal, S., Krivak, T. C., Olawaiye, A. B., and Kanbour-Shakir, A. (2012). Mucinous tumors of the ovary: diagnostic challenges at frozen section and clinical implications. Gynecol Oncol *125*, 75-79.

Taganov, K. D., Boldin, M. P., Chang, K. J., and Baltimore, D. (2006). NF-kappaB-dependent induction of microRNA miR-146, an inhibitor targeted to signaling proteins of innate immune responses. Proc Natl Acad Sci U S A *103*, 12481-12486.

Tothill, R. W., Tinker, A. V., George, J., Brown, R., Fox, S. B., Lade, S., Johnson, D. S., Trivett, M. K., Etemadmoghadam, D., Locandro, B.*, et al.* (2008). Novel molecular subtypes of serous and endometrioid ovarian cancer linked to clinical outcome. Clinical cancer research : an official journal of the American Association for Cancer Research *14*, 5198-5208.

Tournigand, C., Louvet, C., Molitor, J. L., Fritel, X., Dehni, N., Sezeur, A., Pigne, A., Cady, J., Milliez, J., and de Gramont, A. (2003). Long-term survival with consolidation intraperitoneal chemotherapy for patients with advanced ovarian cancer with pathological complete remission. Gynecol Oncol *91*, 341-345.

Tryndyak, V. P., Beland, F. A., and Pogribny, I. P. (2010). E-cadherin transcriptional down-regulation by epigenetic and microRNA-200 family alterations is related to mesenchymal and drug-resistant phenotypes in human breast cancer cells. International journal of cancer Journal international du cancer *126*, 2575-2583.

van Jaarsveld, M. T., Helleman, J., Boersma, A. W., van Kuijk, P. F., van Ijcken, W. F., Despierre, E., Vergote, I., Mathijssen, R. H., Berns, E. M., Verweij, J.*, et al.* (2012). miR-141 regulates KEAP1 and modulates cisplatin sensitivity in ovarian cancer cells. Oncogene.

Vang, S., Wu, H. T., Fischer, A., Miller, D. H., Maclaughlan, S., Douglass, E., Steinhoff, M., Collins, C., Smith, P. J., Brard, L., and Brodsky, A. S. (2013). Identification of Ovarian Cancer Metastatic miRNAs. PloS one *8*, e58226.

Varras, M. N., Sourvinos, G., Diakomanolis, E., Koumantakis, E., Flouris, G. A., Lekka-Katsouli, J., Michalas, S., and Spandidos, D. A. (1999). Detection and clinical correlations of ras gene mutations in human ovarian tumors. Oncology *56*, 89-96.

Vaughan, S., Coward, J. I., Bast, R. C., Berchuck, A., Berek, J. S., Brenton, J. D., Coukos, G., Crum, C. C., Drapkin, R., Etemadmoghadam, D.*, et al.* (2011). Rethinking ovarian cancer: recommendations for improving outcomes. Nat Rev Cancer *11*, 719-725.

Volinia, S., Calin, G. A., Liu, C. G., Ambs, S., Cimmino, A., Petrocca, F., Visone, R., Iorio, M., Roldo, C., Ferracin, M.*, et al.* (2006). A microRNA expression signature of human solid tumors defines cancer gene targets. Proc Natl Acad Sci U S A *103*, 2257-2261.

Wang, T. H., Chan, Y. H., Chen, C. W., Kung, W. H., Lee, Y. S., Wang, S. T., Chang, T. C., and Wang, H. S. (2006). Paclitaxel (Taxol) upregulates expression of functional interleukin-6 in human ovarian cancer cells through multiple signaling pathways. Oncogene *25*, 4857-4866.

Whitehurst, A. W., Bodemann, B. O., Cardenas, J., Ferguson, D., Girard, L., Peyton, M., Minna, J. D., Michnoff, C., Hao, W., Roth, M. G.*, et al.* (2007). Synthetic lethal screen identification of chemosensitizer loci in cancer cells. Nature *446*, 815-819.

Wiegand, K. C., Shah, S. P., Al-Agha, O. M., Zhao, Y., Tse, K., Zeng, T., Senz, J., McConechy, M. K., Anglesio, M. S., Kalloger, S. E.*, et al.* (2010). ARID1A mutations in endometriosis-associated ovarian carcinomas. N Engl J Med *363*, 1532-1543.

Wiklund, E. D., Bramsen, J. B., Hulf, T., Dyrskjot, L., Ramanathan, R., Hansen, T. B., Villadsen, S. B., Gao, S., Ostenfeld, M. S., Borre, M.*, et al.* (2011). Coordinated epigenetic repression of the miR-200 family and miR-205 in invasive bladder cancer. International journal of cancer Journal international du cancer *128*, 1327-1334.

Williams, S. A., Maecker, H. L., French, D. M., Liu, J., Gregg, A., Silverstein, L. B., Cao, T. C., Carano, R. A., and Dixit, V. M. (2011). USP1 deubiquitinates ID proteins to preserve a mesenchymal stem cell program in osteosarcoma. Cell *146*, 918-930.

Wolf, C. R., Hayward, I. P., Lawrie, S. S., Buckton, K., McIntyre, M. A., Adams, D. J., Lewis, A. D., Scott, A. R., and Smyth, J. F. (1987). Cellular heterogeneity and drug resistance in two ovarian adenocarcinoma cell lines derived from a single patient. International journal of cancer Journal international du cancer *39*, 695-702.

Wu, C. H., Mao, T. L., Vang, R., Ayhan, A., Wang, T. L., Kurman, R. J., and Shih Ie, M. (2012). Endocervical-type mucinous borderline tumors are related to endometrioid tumors based on mutation and loss of expression of ARID1A. International journal of gynecological pathology : official journal of the International Society of Gynecological Pathologists *31*, 297-303.

Xie, Y., Wang, X., and Story, M. (2009). Statistical methods of background correction for Illumina BeadArray data. Bioinformatics *25*, 751-757.

Xue, Y., Ouyang, K., Huang, J., Zhou, Y., Ouyang, H., Li, H., Wang, G., Wu, Q., Wei, C., Bi, Y.*, et al.* (2013). Direct conversion of fibroblasts to neurons by reprogramming PTB-regulated microRNA circuits. Cell *152*, 82-96.

Yajima, H., Motohashi, N., Ono, Y., Sato, S., Ikeda, K., Masuda, S., Yada, E., Kanesaki, H., Miyagoe-Suzuki, Y., Takeda, S., and Kawakami, K. (2010). Six family genes control the

proliferation and differentiation of muscle satellite cells. Experimental cell research *316*, 2932-2944.

Yamashita, J., Iwakiri, T., Fukushima, S., Jinnin, M., Miyashita, A., Hamasaki, T., Makino, T., Aoi, J., Masuguchi, S., Inoue, Y., and Ihn, H. (2013). The rs2910164 G>C polymorphism in microRNA-146a is associated with the incidence of malignant melanoma. Melanoma research *23*, 13-20.

Yang, D., Sun, Y., Hu, L., Zheng, H., Ji, P., Pecot, C. V., Zhao, Y., Reynolds, S., Cheng, H., Rupaimoole, R.*, et al.* (2013). Integrated analyses identify a master microRNA regulatory network for the mesenchymal subtype in serous ovarian cancer. Cancer cell *23*, 186-199.

Yi, R., Qin, Y., Macara, I. G., and Cullen, B. R. (2003). Exportin-5 mediates the nuclear export of pre-microRNAs and short hairpin RNAs. Genes & development *17*, 3011-3016.

Yoshitomi, T., Kawakami, K., Enokida, H., Chiyomaru, T., Kagara, I., Tatarano, S., Yoshino, H., Arimura, H., Nishiyama, K., Seki, N., and Nakagawa, M. (2011). Restoration of miR-517a expression induces cell apoptosis in bladder cancer cell lines. Oncology reports *25*, 1661-1668.

Yu, D., Pendergraff, H., Liu, J., Kordasiewicz, H. B., Cleveland, D. W., Swayze, E. E., Lima, W. F., Crooke, S. T., Prakash, T. P., and Corey, D. R. (2012). Single-stranded RNAs use RNAi to potently and allele-selectively inhibit mutant huntingtin expression. Cell *150*, 895-908.

Zaino, R. J., Brady, M. F., Lele, S. M., Michael, H., Greer, B., and Bookman, M. A. (2011). Advanced stage mucinous adenocarcinoma of the ovary is both rare and highly lethal: a Gynecologic Oncology Group study. Cancer *117*, 554-562.

Zeng, Y., Yi, R., and Cullen, B. R. (2003). MicroRNAs and small interfering RNAs can inhibit mRNA expression by similar mechanisms. Proc Natl Acad Sci U S A *100*, 9779-9784.

Zhang, L., Li, J., Young, L. H., and Caplan, M. J. (2006). AMP-activated protein kinase regulates the assembly of epithelial tight junctions. Proc Natl Acad Sci U S A *103*, 17272-17277.

Zhang, L., Volinia, S., Bonome, T., Calin, G. A., Greshock, J., Yang, N., Liu, C. G., Giannakakis, A., Alexiou, P., Hasegawa, K.*, et al.* (2008). Genomic and epigenetic alterations deregulate microRNA expression in human epithelial ovarian cancer. Proc Natl Acad Sci U S A *105*, 7004-7009.

Zhao, J. L., Rao, D. S., Boldin, M. P., Taganov, K. D., O'Connell, R. M., and Baltimore, D. (2011). NF-kappaB dysregulation in microRNA-146a-deficient mice drives the development of myeloid malignancies. Proc Natl Acad Sci U S A *108*, 9184-9189.

Zheng, F., Liao, Y. J., Cai, M. Y., Liu, Y. H., Liu, T. H., Chen, S. P., Bian, X. W., Guan, X. Y., Lin, M. C., Zeng, Y. X.*, et al.* (2012). The putative tumour suppressor microRNA-124 modulates hepatocellular carcinoma cell aggressiveness by repressing ROCK2 and EZH2. Gut *61*, 278-289.